Available online at www.sciencedirect.com
ScienceDirect
International Journal of Solids and Structures 44 (2007) 2244–2268
INTERNATIONAL JOURNAL OF SOLIDS and STRUCTURES
www.elsevier.com/locate/ijsolstr

Consistently linearized constitutive equations of micromechanical models for fibre composites with evolving damage

A. Matzenmiller *, B. Köster

University of Kassel, Institute of Mechanics, D-34109 Kassel, Germany

Received 24 March 2006; received in revised form 23 June 2006
Available online 13 July 2006

Abstract

The numerical analysis of engineering structures is usually based upon the assumptions of a homogeneous as well as a continuous medium. These simplifications are maintained also for structures made of fibre reinforced composite materials which possess by definition a heterogeneous finescale architecture. Furthermore in the course of the loading of such structures void nucleations might arise out of the debonding of the embedded fibres or the growth of microcracks inside the matrix phase. Hence, the assumption of a continuous and homogeneous medium is not valid from a microscopical point of view. Nevertheless, it is numerically advantageous to keep up these simplifying assumptions on the macrolevel. Therefore, the knowledge of the so called macroscopic or effective material behaviour is needed. The overall properties can be described in terms of volume averaged quantities that smear the heterogeneities of the microscopic structure and the influence of its defects. Since the evolution of damage within composite materials means a rather complex process, a purely phenomenological approach is hardly feasible. Hence, the average properties are to be obtained from a micromechanical analysis of the discontinuous and damaged finescale structure. The efficiently reformulated version of the micromechanically based *Generalized Method of Cells* (GMC) provides the macroscopic tangential constitutive tensor in closed-form. The numerical efficiency of the approach allows for the use of the GMC as the constitutive model for nonlinear finite element analyses. Two-scale simulations of macroscale composite structures considering process depending damage evolution on the microscale of heterogeneous media becomes feasible.

Keywords: Composites; Homogenization; Micromechanics; Method of cells; Interface models

1. Introduction

The central objective of this paper is to present a numerically efficient algorithm for obtaining sufficiently reliable predictions of the overall constitutive behaviour of unidirectionally fibre reinforced composite

* Corresponding author.
E-mail address: amat@ifm.maschinenbau.uni-kassel.de (A. Matzenmiller).

0020-7683/$ - see front matter © 2006 Elsevier Ltd. All rights reserved.
doi:10.1016/j.ijsolstr.2006.07.002

materials. The highly nonlinear, irreversible and anisotropic course of damage processes, as it is typically found for composites, is difficult to be described on a purely phenomenological basis. Therefore, use is made of a computational, micromechanically based approach, originally proposed by Aboudi (1991), which is known as the *Generalized Method of Cells* (GMC). The numerical effort of the GMC was reasonably reduced by Pindera and Bednarcyk (1999) using the degrees of freedom of the discretised microscopic stress field as the basic unknowns instead of those of the microscopic strain field. More accurate resolutions of the microfields of stresses and strains are obtainable by the recently published High-Fidelity-GMC (HFGMC), resting on the principle of asymptotic homogenization, see e.g. Aboudi et al. (2002), Aboudi and Pindera (2004), Bednarcyk et al. (2004) or Bansal and Pindera (2005). While the original GMC only applies piecewise linear functions to approximate the microscopic displacement field, the high fidelity approach applies higher order polynomials. The enhanced accuracy of HFGMC is paid with an appreciable increase of computational effort. Since the nonlinear homogenization procedure has to be carried out for each grid point of numerical integration and at each time step during the finite element analysis of composite structures considering process depending damage evolution, the authors stick to the efficient formulation of the GMC for the time being. An approach similar to the one presented here is pursued by Lissenden (1999), who uses the GMC to predict the nonlinear stress responses of metal matrix composites with interfacial decohesion. The model of Lissenden is portrayed in a more rigorous way introducing an evolving internal variable as a functional of the loading history at the interface. In addition the current paper approximates the softening of the epoxy resin by discrete cracks along predeterminate element boundaries of the cells model.

The central aspect of the paper is to present the tangential, homogeneous constitutive tensor of the composite material in conjunction with softening interface models. The tangential stiffness matrix is deduced analytically from the nonlinear equations of the GMC-model. This special derivation of the homogenized tangential stiffness matrix has not been presented before. The process depending macroscopic stiffness matrix is required, if the GMC approach is used as the constitutive model for the finite element analyses of composite structures.

Within the framework of the reformulated GMC unidirectionally reinforced composites, possessing a periodical microstructure, are considered. Due to this restriction the microstructure can be generated by stringing together a sequence of unit cells, consisting of a single fibre, embedded into the surrounding matrix material, see Fig. 1. The generic unit cell is regarded as a representative volume element (RVE) of the heterogeneous medium. The RVE is subdivided into rectangular subdomains which are referred to as the subcells of the unit cell. The microscopic displacement field within the RVE is then approximated by linear functions within each subcell individually. The stress tensors of the subcells are gained from the local displacement fields and the constitutive tensors of the phases. The continuity of tractions is ensured along all subcell interfaces. Displacement discontinuities are conceded to arise at the common boundaries of neighbouring fibre and matrix subcells in order to model an imperfect bond of the phases. Furthermore, selected interfaces between adjacent

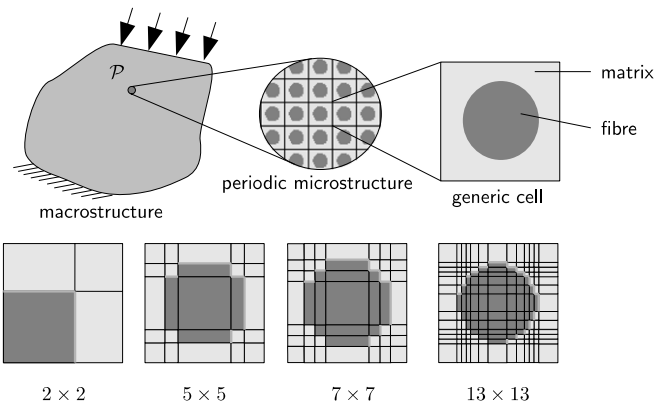

Fig. 1. Top: Macroscopic material point $\mathscr{P}$. Assumed periodical microstructure procreated by a generic cell containing a single fibre. Bottom: Possible discretisations of the generic unit cell by the GMC applying an increasing number of subcells.

matrix cells will serve as localisations for the initiation and growth of crack surfaces within the matrix phase. The continuity conditions imposed on the microfields of stresses and displacements in conjunction with the constitutive equations of the interface models lead to a system of nonlinear algebraic equations.

Those governing equations of the micromechanical model as well as the components of the macroscopic tangential constitutive tensor are derived initially in a general sense independently from the specific interface model under consideration. The only limiting assumption to be fulfilled by the model applied is that the bonding tractions can be expressed in terms of the displacement discontinuities at each interfacial point not excluding their dependency on some additional internal variables. Therewith, it is possible to implement a variety of interface descriptions easily. Among others there may be mentioned the models of Needleman (1987, 1991), Tvergard (1990), Lissenden (1996) or Chaboche et al. (1997) . All these models have in common a certain finite bond strength and the total loss of the ability to transfer interfacial tractions after the displacement discontinuity has surpassed a distinguished limit point. Matzenmiller and Gerlach (2004) and Matzenmiller and Gerlach (2002) combined the GMC with a viscoelastic interface model in order to take into account the rate dependent flexible bond of glass fibres embedded into a viscoelastic epoxy resin. The irreversible debonding process of the fibres from the matrix phase was modelled on the basis of the GMC by Bednarcyk and Arnold (2000a,b), Aboudi and Herakovich (1996) or Lissenden (1996). Therein, the evolution of averaged macroscopic stresses was predicted for a unit cell subjected to different macroscopic strains. The paper at hand not only exerts the GMC to calculate macroscopic stress responses to macroscopic strain processes, but furthermore gives a rigorous derivation of the effective tangential stiffness tensor in closed-form. This feature predestines the proposed implementation to be used as a constitutive material model within the framework of finite element analyses of composite structures.

2. Micromechanics

The intention of a microscopic view on inhomogeneous media is the analytical determination of the effective, averaged material properties of an equivalent, homogeneous substitute material, based on the mechanical properties of the components, their volume fractions and bonding behaviour. The micromechanical modelling of composites is founded on the concept of a representative volume element (RVE). The RVE is defined as the spatial subarea of the heterogeneous medium, which is structurally typical for the whole of the composite. Therefore, it should be large compared to the characteristic lengthscale of the microstructure and small compared to the size of the macrostructure.

The transition from the micro to the macrolevel is done by averaging the microfields of stresses and strains over the volume of the RVE. Hence, the field variables of a macroscopic material point $\mathscr{P}$ are given by the corresponding volume averaged quantities of the microstructural RVE:

$$\langle \boldsymbol{\sigma} \rangle = \frac{1}{V_{\mathrm{RVE}}} \int_{V_{\mathrm{RVE}}} \boldsymbol{\sigma}\, \mathrm{d}V \quad \text{and} \quad \langle \boldsymbol{\epsilon} \rangle = \frac{1}{V_{\mathrm{RVE}}} \int_{V_{\mathrm{RVE}}} \boldsymbol{\epsilon}\, \mathrm{d}V \tag{1}$$

The mathematical relation between these average quantities is set up by the fourth order effective tensor $\mathbb{C}^*$:

$$\langle \boldsymbol{\sigma} \rangle = \mathbb{C}^* : \langle \boldsymbol{\epsilon} \rangle \tag{2}$$

The introduction of Hill's phase averaged concentration tensors $\mathbb{A}^{(i)}$ – see Hill (1963) – constitutes an important basis of micromechanics of elastic materials. By the help of these fourth order tensors the average strain tensors $\langle \boldsymbol{\epsilon}^{(i)} \rangle$ of the individual phases (i) are given as a function of the composite strains $\langle \boldsymbol{\epsilon} \rangle$:

$$\langle \boldsymbol{\epsilon}^{(i)} \rangle = \mathbb{A}^{(i)} : \langle \boldsymbol{\epsilon} \rangle \tag{3}$$

By means of the constitutive tensors $\mathbb{C}^{(i)}$, which are assumed to be constant within each phase, the averaged phase stresses $\langle \boldsymbol{\sigma}^{(i)} \rangle$ can be computed. By introducing the dimensionless volume fractions $c^{(i)} = V^{(i)}/V_{\mathrm{RVE}}$ of the N different phases, the composite stress tensor $\langle \boldsymbol{\sigma} \rangle$ can be calculated from the weighted sum of the averaged phase stresses $\langle \boldsymbol{\sigma}^{(i)} \rangle$:

$$\langle \boldsymbol{\sigma} \rangle = \sum_{i=1}^{N} c^{(i)} \mathbb{C}^{(i)} : \mathbb{A}^{(i)} : \langle \boldsymbol{\epsilon} \rangle \rightarrow \mathbb{C}^* := \sum_{i=1}^{N} c^{(i)} \mathbb{C}^{(i)} : \mathbb{A}^{(i)} \tag{4}$$

In the case of a nonlinear bonding behaviour or the nascency and evolution of cracks, the average phase strain $\langle \boldsymbol{\epsilon}^{(i)} \rangle$ is a nonlinear process dependent tensor functional of the macroscopic strain tensor $\langle \boldsymbol{\epsilon} \rangle$:

$$\langle \boldsymbol{\epsilon}^{(i)} \rangle := \mathscr{G}^{(i)}[\langle \boldsymbol{\epsilon} \rangle] \tag{5}$$

The calculation of the rate of Eq. (5) leads to the definition of a tangential concentration tensor $\tilde{\mathbb{A}}^{(i)}$

$$\frac{\mathrm{d}}{\mathrm{d}t}\mathscr{G}^{(i)} = \langle \dot{\boldsymbol{\epsilon}}^{(i)} \rangle = \frac{\partial \mathscr{G}^{(i)}}{\partial \langle \boldsymbol{\epsilon} \rangle} \frac{\partial \langle \boldsymbol{\epsilon} \rangle}{\partial t} := \tilde{\mathbb{A}}^{(i)} : \langle \dot{\boldsymbol{\epsilon}} \rangle \tag{6}$$

Since the individual phases (i) are still considered to be linear elastic in this paper, the rate of the average stress tensor can be calculated from

$$\langle \dot{\boldsymbol{\sigma}} \rangle = \sum_{i=1}^{N} c^{(i)} \mathbb{C}^{(i)} : \tilde{\mathbb{A}}^{(i)} : \langle \dot{\boldsymbol{\epsilon}} \rangle \rightarrow \tilde{\mathbb{C}}^{*} := \sum_{i=1}^{N} c^{(i)} \mathbb{C}^{(i)} : \tilde{\mathbb{A}}^{(i)} \tag{7}$$

The tangential effective tensor $\tilde{\mathbb{C}}^{*}$ sets up the relation between the rates of the macroscopic strain and stress tensors:

$$\langle \dot{\boldsymbol{\sigma}} \rangle = \tilde{\mathbb{C}}^{*} : \langle \dot{\boldsymbol{\epsilon}} \rangle \tag{8}$$

Hence, the central objective of the micromechanical modelling of damage is to determine the tangential concentration tensors $\tilde{\mathbb{A}}^{(i)}$ in order to evaluate Eq. (7).

2.1. The generalized method of cells

One of the fundamental assumptions of the GMC states that the microstructure is built up by double periodically arranged fibres of infinite length embedded into a surrounding homogeneous matrix phase. Hence, the generic unit cell of the heterogeneous composite consists of a portion of the matrix material, containing a single fibre, see Fig. 1. As a consequence of this basic assumption the unit cell can be regarded as a representative volume element of the composite material.

The location of the macroscopic material point $\mathscr{P}$ is given with regard to a cartesian coordinate system $\mathbf{x}$ which is orientated such that the direction of the x_1-axis coincides with the direction of the perfectly aligned fibres, see Fig. 2. A transversal plane perpendicular to the fibres is spanned by the x_2- and x_3-axes. Subsequently, the microstructure is modelled by subdividing the transversal cross section of the unit cell into $N_\beta \times N_\gamma$ rectangular subcells of which each one is addressed by $(\beta\gamma)$. The total spatial extension of the unit cell in x_2-direction is denoted by h and in x_3-direction by l. The height of the subcell $(\beta\gamma)$ is given by h_β and its width by l_γ. Due to the fact that the fibres are assumed to be perfectly aligned and of infinite length, there is no change of the fine scale architecture in fibre direction. Within the theory of the GMC it holds for

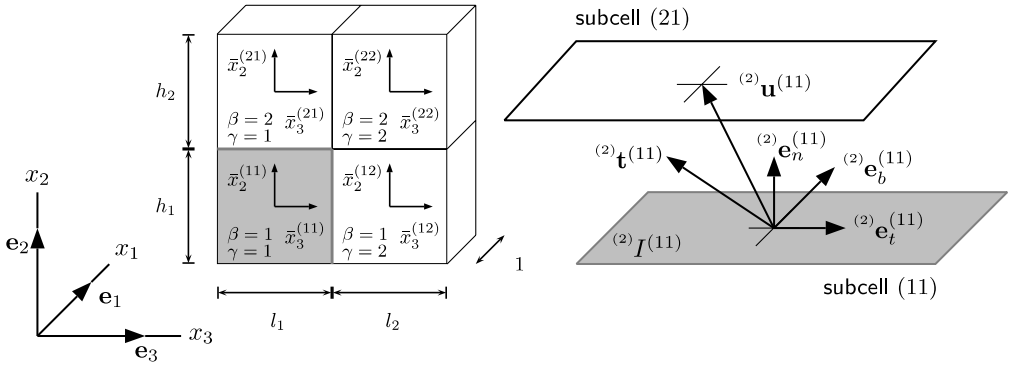

Fig. 2. Left: Coarse model of the original method of cells (MOC), consisting of four subcells and two fibre/matrix-interfaces. Right: Imperfect bond of subcells (11) and (21): traction vector $^{(2)}\mathbf{t}^{(11)}$ and displacement jump vector $^{(2)}\mathbf{u}^{(11)}$.

such a material that the model predictions are not affected by the number of subcells in fibre direction. Hence, the choice of one subcell in fibre direction is sufficient and the length of the cells may be set to unity.

In order to identify the subcell interfaces as well as the related quantities uniquely, we stipulate the following notations. Due to the described discretisation of the unit cell all planar surfaces of the cubic subcells are oriented perpendicular to the macroscopic coordinate system, that is the six outward normal vectors of each subcell domain are directed parallel to the positive or negative x_i-axes, respectively. Now an arbitrary surface I of subcell $(\beta\gamma)$ with an outward normal parallel to the positive x_i-axis is referred to as ${}^{(i)}I^{(\beta\gamma)}$. All appearing interface parameters and variables will be indicated in the same manner, i.e. they will be indexed with two superscripts ${}^{(i)}()^{(\beta\gamma)}$. Whereas the quantities of the subcell $(\beta\gamma)$ itself will be denoted by a single superscript $()^{(\beta\gamma)}$.

The microscopic displacement field $\mathbf{u}$ is approximated piecewisely by linear functions $u_i^{(\beta\gamma)}$ of the local coordinates $\bar{\mathbf{x}}^{(\beta\gamma)}$ within each subcell:

$$u_i^{(\beta\gamma)} = w_i^{(\beta\gamma)} + \bar{x}_2^{(\beta)}\phi_i^{(\beta\gamma)} + \bar{x}_3^{(\gamma)}\psi_i^{(\beta\gamma)}, \quad i = 1,2,3 \tag{9}$$

wherein the quantities $w_i^{(\beta\gamma)}$ describe the translations of the local coordinate systems $\bar{\mathbf{x}}^{(\beta\gamma)}$ attached to the centre of each subcell. The microvariables $\phi_i^{(\beta\gamma)}$ and $\psi_i^{(\beta\gamma)}$ determine the linear expansions of the displacement field throughout the subcell. By making use of the abbreviations

$$\partial_1 := \frac{\partial}{\partial x_1} = \frac{\partial}{\partial \bar{x}_1}, \quad \partial_2 := \frac{\partial}{\partial \bar{x}_2} \quad \text{and} \quad \partial_3 := \frac{\partial}{\partial \bar{x}_3} \tag{10}$$

the displacement functions (9) are derivated with respect to the local coordinate systems to obtain the coordinates of the infinitesimal subcell strain tensor:

$$\epsilon_{ij}^{(\beta\gamma)} = \frac{1}{2}(\partial_i u_j^{(\beta\gamma)} + \partial_j u_i^{(\beta\gamma)}) \tag{11}$$

The displacement field is assumed to be piecewise linear. Hence, the resulting strains are constant throughout the subcell and must be equal to the volume averaged subcell strains in each cell with the volume $V^{(\beta\gamma)}$:

$$\langle \epsilon_{ij}^{(\beta\gamma)} \rangle = \frac{1}{V^{(\beta\gamma)}} \int_{V^{\beta\gamma}} \epsilon_{ij}^{(\beta\gamma)} \, \mathrm{d}V = \epsilon_{ij}^{(\beta\gamma)} \tag{12}$$

The components of the subcell strain tensors, just obtained, are written in vector form in order to make use of Voigt's notation:

$$\langle \underline{\boldsymbol{\epsilon}}^{(\beta\gamma)} \rangle = \{ \langle \epsilon_{11}^{(\beta\gamma)} \rangle \langle \epsilon_{22}^{(\beta\gamma)} \rangle \langle \epsilon_{33}^{(\beta\gamma)} \rangle \langle \epsilon_{23}^{(\beta\gamma)} \rangle \langle \epsilon_{31}^{(\beta\gamma)} \rangle \langle \epsilon_{12}^{(\beta\gamma)} \rangle \}^{\mathrm{T}} \tag{13}$$

The material properties of the phases enter the model by assigning the matrix representations of the constitutive tensors to the corresponding subcells, i.e. we set $\mathbf{C}^{(\beta\gamma)} = \mathbf{C}_{\mathrm{fibre}}$ for the fibre cells and $\mathbf{C}^{(\beta\gamma)} = \mathbf{C}_{\mathrm{matrix}}$ for all matrix cells.

With the stiffness matrices of the phases being given, the average subcell stress tensor is expressed in vector notation:

$$\langle \underline{\boldsymbol{\sigma}}^{(\beta\gamma)} \rangle = \{ \langle \sigma_{11}^{(\beta\gamma)} \rangle \langle \sigma_{22}^{(\beta\gamma)} \rangle \langle \sigma_{33}^{(\beta\gamma)} \rangle \langle \sigma_{23}^{(\beta\gamma)} \rangle \langle \sigma_{31}^{(\beta\gamma)} \rangle \langle \sigma_{21}^{(\beta\gamma)} \rangle \}^{\mathrm{T}} \tag{14}$$

and is computed immediately from the assumption of linear elasticity:

$$\langle \underline{\boldsymbol{\sigma}}^{(\beta\gamma)} \rangle = \underline{\underline{\mathbf{C}}}^{(\beta\gamma)} \langle \underline{\boldsymbol{\epsilon}}^{(\beta\gamma)} \rangle \tag{15}$$

The stress and displacement fields have to fulfil simplified equilibrium and continuity conditions at all subcell boundaries. The continuity of the displacement field is formulated in terms of the surface averaged local displacement functions given by Eq. (9) of two adjacent subcells. This leads to

$${}^{(2)}[\![u_j]\!]^{(\beta\gamma)} = \int_{-l_\gamma/2}^{l_\gamma/2} \int_{-1/2}^{+1/2} u_j^{(\hat{\beta}\gamma)}|_{\bar{x}_2^{(\hat{\beta})} = -h_{\hat{\beta}}/2} \, \mathrm{d}x_1 \, \mathrm{d}\bar{x}_3^{(\hat{\beta}\gamma)} = -\int_{-l_\gamma/2}^{l_\gamma/2} \int_{-1/2}^{+1/2} u_j^{(\beta\gamma)}|_{\bar{x}_2^{(\beta)} = h_\beta/2} \, \mathrm{d}x_1 \, \mathrm{d}\bar{x}_3^{(\beta\gamma)} \tag{16}$$

with $\hat{\beta} = \beta + 1$ and $j = 1,2,3$ for interfaces ${}^{(2)}I^{(\beta\gamma)}$ and to

$$ {}^{(3)}[\![u_j]\!]^{(\beta\gamma)} = \int_{-h_\beta/2}^{h_\beta/2} \int_{-1/2}^{+1/2} u_j^{(\beta\hat{\gamma})}|_{\bar{x}_3^{(\hat{\gamma})} = -l_{\hat{\gamma}}/2} \, \mathrm{d}x_1 \, \mathrm{d}\bar{x}_2^{(\beta\hat{\gamma})} = - \int_{-h_\beta/2}^{h_\beta/2} \int_{-1/2}^{+1/2} u_j^{(\beta\gamma)}|_{\bar{x}_3^{(\gamma)} = l_\gamma/2} \, \mathrm{d}x_1 \, \mathrm{d}\bar{x}_2^{(\beta\gamma)} \tag{17} $$

with $\hat{\gamma} = \gamma + 1$ and $j = 1,2,3$ for interfaces ${}^{(3)}I^{(\beta\gamma)}$. The discontinuities ${}^{(i)}[\![u_j]\!]^{(\beta\gamma)}$ have to vanish for all fibre/fibre subcell interfaces and those matrix/matrix interfaces that do not serve as crack surfaces. The three discontinuities ${}^{(i)}[\![u_j]\!]^{(\beta\gamma)}$ of the interface ${}^{(i)}I^{(\beta\gamma)}$ are compiled by the jump vector

$$ {}^{(i)}\mathbf{u}^{(\beta\gamma)} = {}^{(i)}[\![u_j]\!]^{(\beta\gamma)} {}^{(i)}\mathbf{e}_j^{(\beta\gamma)} \tag{18} $$

In the subsequent steps all appearing interfacial quantities need to be described in a local basis system. Therefore, we introduce one orthonormal (n,t,b)-coordinate system for each of the imperfectly bonded subcell interfaces as it is indicated for ${}^{(2)}I^{(11)}$ on the right hand side of Fig. 2. The outward normal direction is defined by the unit vector $\mathbf{e}_n$. The plane of the interface itself is given by the two tangential unit vectors $\mathbf{e}_t$ and $\mathbf{e}_b$. By means of Fig. 2 it is given as

$$ {}^{(2)}\mathbf{e}_n^{(\beta\gamma)} \| \mathbf{e}_2, \quad {}^{(2)}\mathbf{e}_t^{(\beta\gamma)} \| \mathbf{e}_3, \quad {}^{(2)}\mathbf{e}_b^{(\beta\gamma)} \| \mathbf{e}_1 \tag{19} $$

and analogously it holds that

$$ {}^{(3)}\mathbf{e}_n^{(\beta\gamma)} \| \mathbf{e}_3, \quad {}^{(3)}\mathbf{e}_t^{(\beta\gamma)} \| \mathbf{e}_1, \quad {}^{(3)}\mathbf{e}_b^{(\beta\gamma)} \| \mathbf{e}_2 \tag{20} $$

Hence, the displacement jump vectors (18) depend on the basis of the local systems as follows:

$$ {}^{(2)}\mathbf{u}^{(\beta\gamma)} = \begin{Bmatrix} {}^{(2)}[\![u_n]\!]^{(\beta\gamma)} \\ {}^{(2)}[\![u_t]\!]^{(\beta\gamma)} \\ {}^{(2)}[\![u_b]\!]^{(\beta\gamma)} \end{Bmatrix} := \begin{Bmatrix} {}^{(2)}[\![u_2]\!]^{(\beta\gamma)} \\ {}^{(2)}[\![u_3]\!]^{(\beta\gamma)} \\ {}^{(2)}[\![u_1]\!]^{(\beta\gamma)} \end{Bmatrix} \tag{21} $$

and

$$ {}^{(3)}\mathbf{u}^{(\beta\gamma)} = \begin{Bmatrix} {}^{(3)}[\![u_n]\!]^{(\beta\gamma)} \\ {}^{(3)}[\![u_t]\!]^{(\beta\gamma)} \\ {}^{(3)}[\![u_b]\!]^{(\beta\gamma)} \end{Bmatrix} := \begin{Bmatrix} {}^{(3)}[\![u_3]\!]^{(\beta\gamma)} \\ {}^{(3)}[\![u_1]\!]^{(\beta\gamma)} \\ {}^{(3)}[\![u_2]\!]^{(\beta\gamma)} \end{Bmatrix} \tag{22} $$

By postulating the continuity of displacements on the basis of Eqs. (16), (17), (21) and (22), the following Eqs. (23)–(28) are induced. The ranges of the subcell indices are $\beta = 1,2,\ldots,N_\beta = \overline{1,N_\beta}$ and $\gamma = 1,2,\ldots,N_\gamma = \overline{1,N\gamma}$. For a detailed derivation see Aboudi (1993).

$$ \langle \epsilon_{11}^{(\beta\gamma)} \rangle = \langle \epsilon_{11} \rangle, \quad \beta = \overline{1,N_\beta}, \quad \gamma = \overline{1,N_\gamma} \tag{23} $$

$$ \sum_{\beta=1}^{N_\beta} h_\beta \langle \epsilon_{22}^{(\beta\gamma)} \rangle + {}^{(2)}[\![u_2]\!]^{(\beta\gamma)} = h\langle \epsilon_{22} \rangle, \quad \gamma = \overline{1,N_\gamma} \tag{24} $$

$$ \sum_{\gamma=1}^{N_\gamma} l_\gamma \langle \epsilon_{33}^{(\beta\gamma)} \rangle + {}^{(3)}[\![u_3]\!]^{(\beta\gamma)} = l\langle \epsilon_{33} \rangle, \quad \beta = \overline{1,N_\beta} \tag{25} $$

$$ \sum_{\beta=1}^{N_\beta} h_\beta \langle \epsilon_{12}^{(\beta\gamma)} \rangle + {}^{(2)}[\![u_1]\!]^{(\beta\gamma)} = h\langle \epsilon_{12} \rangle, \quad \gamma = \overline{1,N_\gamma} \tag{26} $$

$$ \sum_{\beta=1}^{N_\beta} l_\gamma \langle \epsilon_{13}^{(\beta\gamma)} \rangle + {}^{(3)}[\![u_1]\!]^{(\beta\gamma)} = l\langle \epsilon_{13} \rangle, \quad \beta = \overline{1,N_\beta} \tag{27} $$

$$ \sum_{\beta=1}^{N_\beta} \sum_{\gamma=1}^{N_\gamma} h_\beta l_\gamma \langle \epsilon_{23}^{(\beta\gamma)} \rangle + l_\gamma {}^{(2)}[\![u_3]\!]^{(\beta\gamma)} + h_\beta {}^{(3)}[\![u_2]\!]^{(\beta\gamma)} = hl\langle \epsilon_{23} \rangle \tag{28} $$

The equilibrium condition at the cell interfaces requires the continuity of tractions, which is ensured by enforcing the average subcell stresses of neighbouring cells to meet the following equalities:

$$\begin{aligned}
&\langle\sigma_{2j}^{(\beta\gamma)}\rangle = \langle\sigma_{2j}^{(\hat{\beta}\gamma)}\rangle, \quad \gamma = \overline{1,N_\gamma}, \quad \hat{\beta} = \begin{cases} \beta+1, & \beta < N_\beta \\ 1, & \beta = N_\beta \end{cases} \\
&\langle\sigma_{3j}^{(\beta\gamma)}\rangle = \langle\sigma_{3j}^{(\beta\hat{\gamma})}\rangle, \quad \beta = \overline{1,N_\beta}, \quad \hat{\gamma} = \begin{cases} \gamma+1, & \gamma < N_\gamma \\ 1, & \gamma = N_\gamma \end{cases}
\end{aligned} \tag{29}$$

The stress continuity equations (29) enforce piecewisely uniform microstress fields throughout the cells model of the RVE. Since those subcell clusters, supporting the (spatial) constant stresses, are determined a priori by Eq. (29), the following mesostress quantities T_{ij} are defined by Pindera and Bednarcyk (1999):

$$\begin{aligned}
T_{21}^{(\gamma)} &:= \langle\sigma_{21}^{(1\gamma)}\rangle = \langle\sigma_{21}^{(2\gamma)}\rangle = \cdots = \langle\sigma_{21}^{(N_\beta\gamma)}\rangle, \quad \gamma = \overline{1,N_\gamma} \\
T_{22}^{(\gamma)} &:= \langle\sigma_{22}^{(1\gamma)}\rangle = \langle\sigma_{22}^{(2\gamma)}\rangle = \cdots = \langle\sigma_{22}^{(N_\beta\gamma)}\rangle, \quad \gamma = \overline{1,N_\gamma} \\
T_{23}^{(\gamma)} &:= \langle\sigma_{23}^{(1\gamma)}\rangle = \langle\sigma_{23}^{(2\gamma)}\rangle = \cdots = \langle\sigma_{23}^{(N_\beta\gamma)}\rangle, \quad \gamma = \overline{1,N_\gamma} \\
T_{33}^{(\beta)} &:= \langle\sigma_{33}^{(\beta 1)}\rangle = \langle\sigma_{33}^{(\beta 2)}\rangle = \cdots = \langle\sigma_{33}^{(\beta N_\gamma)}\rangle, \quad \beta = \overline{1,N_\beta} \\
T_{31}^{(\beta)} &:= \langle\sigma_{31}^{(\beta 1)}\rangle = \langle\sigma_{31}^{(\beta 2)}\rangle = \cdots = \langle\sigma_{31}^{(\beta N_\gamma)}\rangle, \quad \beta = \overline{1,N_\beta} \\
T_{32}^{(\beta)} &:= \langle\sigma_{32}^{(\beta 1)}\rangle = \langle\sigma_{32}^{(\beta 2)}\rangle = \cdots = \langle\sigma_{32}^{(\beta N_\gamma)}\rangle, \quad \beta = \overline{1,N_\beta}
\end{aligned} \tag{30}$$

The variables T_{ij} stand for the average stresses in the subcell rows β and columns γ, respectively. Due to the symmetry of the stress tensor a further identification of stresses follows from Eqs. $(30)_3$ and $(30)_6$, namely

$$T_{23} := T_{23}^{(\gamma)} = T_{32}^{(\beta)} \tag{31}$$

for all arbitrary pairings of β and γ. Finally, the stresses $T_{11}^{(\beta\gamma)} := \langle\sigma_{11}^{(\beta\gamma)}\rangle$ are introduced in order to unify the further on notations. Hence, the total number of stress variables T_{ij} amounts to $N_\beta N_\gamma + 2(N_\beta + N_\gamma) + 1$, which equals to the total count of displacement relations (23)–(28). By assuming a linear elastic constitutive behaviour for each component of the composite, i.e.

$$\langle\epsilon_{ij}^{(\beta\gamma)}\rangle = S_{ijkl}^{(\beta\gamma)}\langle\sigma_{kl}^{(\beta\gamma)}\rangle \tag{32}$$

the subcell strains $\langle\epsilon_{ij}^{(\beta\gamma)}\rangle$ in Eqs. (23)–(28) can be replaced by the subcell stresses $\langle\sigma_{ij}^{(\beta\gamma)}\rangle$ and compliances $S_{ijkl}^{(\beta\gamma)}$ as it will be deduced next. The constitutive Eq. (32) reads in vector–matrix-notation as

$$\langle\underline{\boldsymbol{\epsilon}}^{(\beta\gamma)}\rangle = \underline{\underline{\mathbf{S}}}^{(\beta\gamma)}\langle\underline{\boldsymbol{\sigma}}^{(\beta\gamma)}\rangle \Longleftrightarrow \begin{Bmatrix} \langle\epsilon_{11}^{(\beta\gamma)}\rangle \\ \langle\epsilon_{22}^{(\beta\gamma)}\rangle \\ \langle\epsilon_{33}^{(\beta\gamma)}\rangle \\ \langle\epsilon_{23}^{(\beta\gamma)}\rangle \\ \langle\epsilon_{31}^{(\beta\gamma)}\rangle \\ \langle\epsilon_{21}^{(\beta\gamma)}\rangle \end{Bmatrix} = \begin{bmatrix} \mathsf{S}_{11}^{(\beta\gamma)} & \mathsf{S}_{12}^{(\beta\gamma)} & \mathsf{S}_{13}^{(\beta\gamma)} & 0 & 0 & 0 \\ \mathsf{S}_{21}^{(\beta\gamma)} & \mathsf{S}_{22}^{(\beta\gamma)} & \mathsf{S}_{23}^{(\beta\gamma)} & 0 & 0 & 0 \\ \mathsf{S}_{31}^{(\beta\gamma)} & \mathsf{S}_{32}^{(\beta\gamma)} & \mathsf{S}_{33}^{(\beta\gamma)} & 0 & 0 & 0 \\ 0 & 0 & 0 & \mathsf{S}_{44}^{(\beta\gamma)} & 0 & 0 \\ 0 & 0 & 0 & 0 & \mathsf{S}_{55}^{(\beta\gamma)} & 0 \\ 0 & 0 & 0 & 0 & 0 & \mathsf{S}_{66}^{(\beta\gamma)} \end{bmatrix} \begin{Bmatrix} \langle\sigma_{11}^{(\beta\gamma)}\rangle \\ \langle\sigma_{22}^{(\beta\gamma)}\rangle \\ \langle\sigma_{33}^{(\beta\gamma)}\rangle \\ \langle\sigma_{23}^{(\beta\gamma)}\rangle \\ \langle\sigma_{31}^{(\beta\gamma)}\rangle \\ \langle\sigma_{21}^{(\beta\gamma)}\rangle \end{Bmatrix} \tag{33}$$

The entries of the subcell stress vector $\langle\underline{\boldsymbol{\sigma}}^{(\beta\gamma)}\rangle$ in Eq. (33) can be identified with the stresses T_{ij} just defined in Eqs. (30) and (31):

$$\langle\underline{\boldsymbol{\sigma}}^{(\beta\gamma)}\rangle^{\mathrm{T}} = \left\{ \langle\sigma_{11}^{(\beta\gamma)}\rangle \quad \langle\sigma_{22}^{(\beta\gamma)}\rangle \quad \langle\sigma_{33}^{(\beta\gamma)}\rangle \quad \langle\sigma_{23}^{(\beta\gamma)}\rangle \quad \langle\sigma_{31}^{(\beta\gamma)}\rangle \quad \langle\sigma_{21}^{(\beta\gamma)}\rangle \right\} = \left\{ T_{11}^{(\beta\gamma)} \quad T_{22}^{(\gamma)} \quad T_{33}^{(\beta)} \quad T_{23} \quad T_{31}^{(\beta)} \quad T_{21}^{(\gamma)} \right\} \tag{34}$$

Since the method of cells discretises the fibre direction of the RVE with a single subdivision of unit length, all subcell strains $\langle\epsilon_{11}^{(\beta\gamma)}\rangle$ are equal to the macroscopic strain $\langle\epsilon_{11}\rangle$ as it is stated by Eq. (23). Therefore, by combining the first of Eqs. (33) with Eq. (34), it follows immediately:

$$\langle\epsilon_{11}\rangle = \langle\epsilon_{11}^{(\beta\gamma)}\rangle = \mathsf{S}_{11}^{(\beta\gamma)}T_{11}^{(\beta\gamma)} + \mathsf{S}_{12}^{(\beta\gamma)}T_{22}^{(\gamma)} + \mathsf{S}_{13}^{(\beta\gamma)}T_{33}^{(\beta)} \tag{35}$$

The subcell stresses $T_{11}^{(\beta\gamma)}$ are readily obtained from Eq. (35):

$$T_{11}^{(\beta\gamma)} = \frac{1}{S_{11}^{(\beta\gamma)}}\langle\epsilon_{11}\rangle - \frac{S_{12}^{(\beta\gamma)}}{S_{11}^{(\beta\gamma)}}T_{22}^{(\gamma)} - \frac{S_{13}^{(\beta\gamma)}}{S_{11}^{(\beta\gamma)}}T_{33}^{(\beta)}, \quad \beta = \overline{1,N_\beta}, \ \ \gamma = \overline{1,N_\gamma} \tag{36}$$

The strain $\langle\epsilon_{11}\rangle$ in Eq. (36) is part of the given displacement boundary conditions imposed on the RVE. Hence, by utilising the $N_\beta N_\gamma$ displacement conditions (23) to receive the relations (36), the stresses $T_{11}^{(\beta\gamma)}$ have become dependent variables and the number of unknown stresses T_{ij} is accordingly reduced to $N_T = 2(N_\beta + N_\gamma) + 1$. If the constitutive Eq. (33) are considered together with the stresses $T_{11}^{(\beta\gamma)}$ in Eq. (36), the normal strains in the transversal planes are calculated to

$$\langle\epsilon_{22}^{(\beta\gamma)}\rangle = \frac{S_{21}^{(\beta\gamma)}}{S_{11}^{(\beta\gamma)}}\langle\epsilon_{11}\rangle + \left(S_{22}^{(\beta\gamma)} - \frac{S_{21}^{(\beta\gamma)}S_{12}^{(\beta\gamma)}}{S_{11}^{(\beta\gamma)}}\right)T_{22}^{(\gamma)} + \left(S_{23}^{(\beta\gamma)} - \frac{S_{21}^{(\beta\gamma)}S_{13}^{(\beta\gamma)}}{S_{11}^{(\beta\gamma)}}\right)T_{33}^{(\beta)} \tag{37}$$

and

$$\langle\epsilon_{33}^{(\beta\gamma)}\rangle = \frac{S_{31}^{(\beta\gamma)}}{S_{11}^{(\beta\gamma)}}\langle\epsilon_{11}\rangle + \left(S_{32}^{(\beta\gamma)} - \frac{S_{31}^{(\beta\gamma)}S_{12}^{(\beta\gamma)}}{S_{11}^{(\beta\gamma)}}\right)T_{22}^{(\gamma)} + \left(S_{33}^{(\beta\gamma)} - \frac{S_{31}^{(\beta\gamma)}S_{13}^{(\beta\gamma)}}{S_{11}^{(\beta\gamma)}}\right)T_{33}^{(\beta)} \tag{38}$$

Finally, the shear strains of the subcells result from (33) and (34):

$$\langle\epsilon_{23}^{(\beta\gamma)}\rangle = S_{44}^{(\beta\gamma)}T_{23}; \quad \langle\epsilon_{31}^{(\beta\gamma)}\rangle = S_{55}^{(\beta\gamma)}T_{31}^{(\beta)}; \quad \langle\epsilon_{21}^{(\beta\gamma)}\rangle = S_{66}^{(\beta\gamma)}T_{21}^{(\gamma)} \tag{39}$$

Now, the microstrains $\langle\epsilon_{ij}^{(\beta\gamma)}\rangle$ in the continuity conditions (24)–(28) can be substituted by the stresses T_{ij} and the compliances $S_{ij}^{(\beta\gamma)}$ on the basis of Eqs. (37)–(39). By means of the definitions

$$\begin{aligned}
&\overline{S}_{23}^{(\beta\gamma)} := h_\beta\left(S_{23}^{(\beta\gamma)} - \frac{S_{12}^{(\beta\gamma)}S_{13}^{(\beta\gamma)}}{S_{11}^{(\beta\gamma)}}\right); \quad \overline{S}_{22}^{(\gamma)} := \sum_{\beta=1}^{N_\beta} h_\beta\left(S_{22}^{(\beta\gamma)} - \frac{S_{12}^{(\beta\gamma)}S_{12}^{(\beta\gamma)}}{S_{11}^{(\beta\gamma)}}\right)\\
&\overline{S}_{32}^{(\beta\gamma)} := l_\gamma\left(S_{23}^{(\beta\gamma)} - \frac{S_{12}^{(\beta\gamma)}S_{13}^{(\beta\gamma)}}{S_{11}^{(\beta\gamma)}}\right); \quad \overline{S}_{33}^{(\beta)} := \sum_{\gamma=1}^{N_\gamma} l_\gamma\left(S_{33}^{(\beta\gamma)} - \frac{S_{13}^{(\beta\gamma)}S_{13}^{(\beta\gamma)}}{S_{11}^{(\beta\gamma)}}\right)\\
&\overline{S}_{12}^{(\gamma)} := \sum_{\beta=1}^{N_\beta} h_\beta\frac{S_{12}^{(\beta\gamma)}}{S_{11}^{(\beta\gamma)}}; \quad \overline{S}_{13}^{(\beta)} := \sum_{\gamma=1}^{N_\gamma} l_\gamma\frac{S_{13}^{(\beta\gamma)}}{S_{11}^{(\beta\gamma)}}
\end{aligned} \tag{40}$$

and

$$\overline{S}_{44} := \sum_{\beta=1}^{N_\beta}\sum_{\gamma=1}^{N_\gamma} h_\beta l_\gamma S_{44}^{(\beta\gamma)}; \quad \overline{S}_{55}^{(\beta)} := \sum_{\gamma=1}^{N_\gamma} l_\gamma S_{55}^{(\beta\gamma)}; \quad \overline{S}_{66}^{(\gamma)} := \sum_{\beta=1}^{N_\beta} h_\beta S_{66}^{(\beta\gamma)} \tag{41}$$

the reformulated displacement relations (24)–(28) read as follows:

$$h\langle\epsilon_{22}\rangle - \overline{S}_{12}^{(\gamma)}\langle\epsilon_{11}\rangle = \overline{S}_{22}^{(\gamma)}T_{22}^{(\gamma)} + \sum_{\beta=1}^{N_\beta}\overline{S}_{23}^{(\beta\gamma)}T_{33}^{(\beta)} + \sum_{\beta=1}^{N_\beta}{}^{(2)}[\![u_2]\!]^{(\beta\gamma)}, \quad \gamma = \overline{1,N_\gamma} \tag{42}$$

$$l\langle\epsilon_{33}\rangle - \overline{S}_{13}^{(\beta)}\langle\epsilon_{11}\rangle = \overline{S}_{33}^{(\beta)}T_{33}^{(\beta)} + \sum_{\gamma=1}^{N_\gamma}\overline{S}_{32}^{(\beta\gamma)}T_{22}^{(\gamma)} + \sum_{\gamma=1}^{N_\gamma}{}^{(3)}[\![u_3]\!]^{(\beta\gamma)}, \quad \beta = \overline{1,N_\beta} \tag{43}$$

$$h\langle\epsilon_{12}\rangle = \overline{S}_{66}^{(\gamma)}T_{21}^{(\gamma)} + \sum_{\beta=1}^{N_\beta}{}^{(2)}[\![u_1]\!]^{(\beta\gamma)}, \quad \gamma = \overline{1,N_\gamma} \tag{44}$$

$$l\langle\epsilon_{13}\rangle = \overline{S}_{55}^{(\beta)}T_{31}^{(\beta)} + \sum_{\gamma=1}^{N_\gamma}{}^{(3)}[\![u_1]\!]^{(\beta\gamma)}, \quad \beta = \overline{1,N_\beta} \tag{45}$$

$$hl\langle\epsilon_{23}\rangle = \overline{S}_{44}T_{23} + \sum_{\beta=1}^{N_\beta}\sum_{\gamma=1}^{N_\gamma}(l_\gamma{}^{(2)}[\![u_3]\!]^{(\beta\gamma)} + h_\beta{}^{(3)}[\![u_2]\!]^{(\beta\gamma)}) \tag{46}$$

The $N_T = 2(N_\beta + N_\gamma) + 1$ revised Eqs. (42)–(46) are summarised by the matrix expression:

$$\mathbf{S}\mathbf{T} + \mathbf{D}_u\hat{\mathbf{u}} = \mathbf{K}\langle\underline{\boldsymbol{\epsilon}}\rangle \tag{47}$$

Herein, the vector $\mathbf{T}$ contains the N_T unknown stresses T_{ij} ordered as

$$\mathbf{T}^{\mathrm{T}} := \left\{ \begin{array}{lllll} T_{22}^{(\gamma)} \ldots & |T_{33}^{(\beta)} \ldots & |T_{21}^{(\gamma)} \ldots & |T_{31}^{(\beta)} \ldots & |T_{23} \\ \mapsto & \mapsto & \mapsto & \mapsto & \\ \gamma = \overline{1, N_\gamma} & \beta = \overline{1, N_\beta} & \gamma = \overline{1, N_\gamma} & \beta = \overline{1, N_\beta} & \end{array} \right\} \tag{48}$$

The compliance factors defined by the sets of Eqs. (40) and (41) build up the non-symmetric $N_T \times N_T$ matrix $\mathbf{S}$. The $N_T \times 6$ matrix $\mathbf{K}$ is given by the total height h and width l of the unit cell as well as the terms $\overline{S}_{12}^{(\gamma)}$ and $\overline{S}_{13}^{(\beta)}$ given in Eq. (40). The displacement jump vectors ${}^{(i)}\mathbf{u}^{(\beta\gamma)} \neq \mathbf{0}$ for the imperfectly bonded or cracked interfaces considered below are extracted with the incidence matrix $\mathbb{ID}$ from the set of all possible jump discontinuities at all subcell interfaces in order to constitute the hyper vector $\hat{\mathbf{u}}$:

$$\hat{\mathbf{u}} = \mathbb{ID} \begin{bmatrix} {}^{(2)}\mathbf{u}^{(11)} \\ \vdots \\ {}^{(2)}\mathbf{u}^{(N_\beta N_\gamma)} \\ {}^{(3)}\mathbf{u}^{(11)} \\ \vdots \\ {}^{(3)}\mathbf{u}^{(N_\beta N_\gamma)} \end{bmatrix} \tag{49}$$

The incidence matrix $\mathbb{ID}$ is given as an example in Appendix A explicitly for the coarse model in Fig. 2 with four subcells and the two flexible interfaces ${}^{(2)}I^{(11)}$ and ${}^{(3)}I^{(11)}$ between the fibre and matrix cells. Generally, a total number of N_I imperfectly bonded or cracked interfaces is assumed to exist within the RVE, causing the dimension of the resulting hyper vector $\hat{\mathbf{u}}$ to be $3N_I$. The term $\mathbf{D}_u$ in Eq. (47) represents a matrix that allocates the displacement jumps $\hat{\mathbf{u}}$ to the appropriate continuity (42)–(46).

In the case of debonding or matrix cracking another $3N_I$ equations are set up to express the interfacial tractions $\mathbf{t}$ as nonlinear functions $\mathbf{f}$ of the displacement jump vectors

$${}^{(i)}\mathbf{t}^{(\beta\gamma)} = \mathbf{f}({}^{(i)}\mathbf{u}^{(\beta\gamma)}, {}^{(i)}q^{(\beta\gamma)}) \tag{50}$$

and some dependently evolving internal variables q, which will be defined in Section 3 explicitly and computed from process depending functionals $\mathscr{F}_{t\geqslant 0}(t)$:

$${}^{(i)}q^{(\beta\gamma)}(t) := \mathscr{F}({}^{(i)}\mathbf{u}^{(\beta\gamma)}(\tau))_{\tau=0}^{\tau=t} \tag{51}$$

Since the continuity of tractions is claimed across the subcell boundaries, the interfacial traction vectors ${}^{(i)}\mathbf{t}^{(\beta\gamma)}$ of Eq. (50) must be equal to the stress vectors $\langle\boldsymbol{\sigma}^{(\beta\gamma)}\rangle\,{}^{(i)}\mathbf{e}_n^{(\beta\gamma)}$ on the subcell surfaces. They read in matrix notation for the special case of Eqs. (19), (20) and (34) as

$${}^{(2)}\mathbf{t}^{(\beta\gamma)} = \left\{ \begin{array}{l} {}^{(2)}t_n^{(\beta\gamma)} \\ {}^{(2)}t_t^{(\beta\gamma)} \\ {}^{(2)}t_b^{(\beta\gamma)} \end{array} \right\} = \left\{ \begin{array}{l} \langle\sigma_{22}^{(\beta\gamma)}\rangle \\ \langle\sigma_{23}^{(\beta\gamma)}\rangle \\ \langle\sigma_{21}^{(\beta\gamma)}\rangle \end{array} \right\} = \left\{ \begin{array}{l} T_{22}^{(\gamma)} \\ T_{23} \\ T_{21}^{(\gamma)} \end{array} \right\} \tag{52}$$

and

$${}^{(3)}\mathbf{t}^{(\beta\gamma)} = \left\{ \begin{array}{l} {}^{(2)}t_n^{(\beta\gamma)} \\ {}^{(2)}t_t^{(\beta\gamma)} \\ {}^{(2)}t_b^{(\beta\gamma)} \end{array} \right\} = \left\{ \begin{array}{l} \langle\sigma_{33}^{(\beta\gamma)}\rangle \\ \langle\sigma_{31}^{(\beta\gamma)}\rangle \\ \langle\sigma_{32}^{(\beta\gamma)}\rangle \end{array} \right\} = \left\{ \begin{array}{l} T_{33}^{(\beta)} \\ T_{23} \\ T_{31}^{(\beta)} \end{array} \right\} \tag{53}$$

There is one equation (50) for each flexible or cracked interface ${}^{(i)}I^{(\beta\gamma)}$ of the model. In order to render them by a single matrix equation, the following quantities are defined:

$$\hat{\mathbf{t}} := \mathbb{ID}\begin{bmatrix} {}^{(2)}\mathbf{t}^{(11)} \\ \vdots \\ {}^{(2)}\mathbf{t}^{(N_\beta N_\gamma)} \\ {}^{(3)}\mathbf{t}^{(11)} \\ \vdots \\ {}^{(3)}\mathbf{t}^{(N_\beta N_\gamma)} \end{bmatrix}, \quad \hat{\mathbf{f}} := \mathbb{ID}\begin{bmatrix} {}^{(2)}\mathbf{f}^{(11)} \\ \vdots \\ {}^{(2)}\mathbf{f}^{(N_\beta N_\gamma)} \\ {}^{(3)}\mathbf{f}^{(11)} \\ \vdots \\ {}^{(3)}\mathbf{f}^{(N_\beta N_\gamma)} \end{bmatrix}, \quad \hat{\mathbf{q}} := \mathbb{ID}^q\begin{bmatrix} {}^{(2)}q^{(11)} \\ \vdots \\ {}^{(2)}q^{(N_\beta N_\gamma)} \\ {}^{(3)}q^{(11)} \\ \vdots \\ {}^{(3)}q^{(N_\beta N_\gamma)} \end{bmatrix} \tag{54}$$

where $\mathbb{ID}$ is the incidence matrix, already used in Eq. (49) to define $\hat{\mathbf{u}}$. $\mathbb{ID}^q$ is an incidence matrix, given in Appendix A, to form the N_I-dimensional vector $\hat{\mathbf{q}}$ in which all damage variables ${}^{(i)}q^{(\beta\gamma)}$ are stored. Obviously, the hyper vectors $\hat{\mathbf{f}}$ and $\hat{\mathbf{t}}$ possess the same dimension $3N_I$ as the previously defined vector $\hat{\mathbf{u}}$. The hyper vector $\hat{\mathbf{t}}$ comprises all stress vectors on flexible or cracked interfaces. Due to Eqs. (52) and (53) the vector $\hat{\mathbf{t}}$ can also be written as

$$\hat{\mathbf{t}} = \mathbf{D}_T\mathbf{T} \tag{55}$$

by making use of the incidence matrix $\mathbf{D}_T$ that maps the stress vector $\mathbf{T}$ onto the vector $\hat{\mathbf{t}}$. The size of the non-symmetric, non-quadratic matrix $\mathbf{D}_T$ depends on both the number of the $3N_I$ displacement jumps and the number of the N_T stresses $\mathbf{T}$. By using the definitions (54) and (55), the relations (50) can be expressed as a set of nonlinear equations which – together with Eq. (47) – completely describe the micromechanical model mathematically for the unknowns $\mathbf{T}$ and $\hat{\mathbf{u}}$:

$$\begin{aligned} &\mathbf{S}\mathbf{T} + \mathbf{D}_u\hat{\mathbf{u}} = \mathbf{K}\langle\underline{\boldsymbol{\epsilon}}\rangle \\ &\mathbf{D}_T\mathbf{T} - \hat{\mathbf{f}}(\hat{\mathbf{u}}, \hat{\mathbf{q}}) = 0 \end{aligned} \tag{56}$$

The column vector $\hat{\mathbf{q}}$ of the internal variables is determined from the process history of the displacement jumps $\hat{\mathbf{u}}$ – see Eqs. (51). The macroscopic strain $\langle\underline{\boldsymbol{\epsilon}}\rangle$ is usually given as a function of time t and serves in the right hand side as the external process variable for the micromechanical analysis.

2.2. Average stresses and tangential stiffness matrix

After having found the solution $\{\mathbf{T}, \hat{\mathbf{u}}\}$ of the system (56) at a certain point of time, say $t = {}^k t$: the macroscopic stress vector $({}^k\underline{\boldsymbol{\sigma}})$ results from the volume averaged sum of the subcell stresses:

$$\langle\underline{\boldsymbol{\sigma}}\rangle|_{k_t} = \frac{1}{hl}\sum_{\beta=1}^{N_\beta}\sum_{\gamma=1}^{N_\gamma} h_\beta l_\gamma \langle {}^k\underline{\boldsymbol{\sigma}}^{(\beta\gamma)}\rangle \tag{57}$$

Omitting the superscript k for convenience and considering Eqs. (34) and (36), the stress equation (57) merge into

$$\langle\sigma_{11}\rangle = \sum_{\beta=1}^{N_\beta}\sum_{\gamma=1}^{N_\gamma}\frac{h_\beta l_\gamma}{hl}\left[\frac{1}{\mathsf{S}_{11}^{(\beta\gamma)}}\langle\epsilon_{11}\rangle - \frac{\mathsf{S}_{12}^{(\beta\gamma)}}{\mathsf{S}_{11}^{(\beta\gamma)}}T_{22}^{(\gamma)} - \frac{\mathsf{S}_{13}^{(\beta\gamma)}}{\mathsf{S}_{11}^{(\beta\gamma)}}T_{33}^{(\beta)}\right] \tag{58}$$

and

$$\begin{aligned} &\langle\sigma_{22}\rangle = \sum_{\gamma=1}^{N_\gamma}\frac{l_\gamma}{l}T_{22}^{(\gamma)}; \quad \langle\sigma_{33}\rangle = \sum_{\beta=1}^{N_\beta}\frac{h_\beta}{h}T_{33}^{(\beta)}; \\ &\langle\sigma_{21}\rangle = \sum_{\gamma=1}^{N_\gamma}\frac{l_\gamma}{l}T_{21}^{(\gamma)}; \quad \langle\sigma_{31}\rangle = \sum_{\beta=1}^{N_\beta}\frac{h_\beta}{h}T_{31}^{(\beta)}; \quad \langle\sigma_{23}\rangle = T_{23} \end{aligned} \tag{59}$$

In order to use the GMC as a constitutive model for the finite element analyses of engineering structures, the homogenized tangential stiffness of the composite material is required in addition to the macrostress responses. The derivation of the stiffness matrix in conjunction with softening interface models has not yet been given. It is deduced here for the efficiently reformulated version of the GMC. The actual rate of the macrostress $\langle\underline{\boldsymbol{\sigma}}\rangle$ at time ${}^{k}t$ reads

$$\left.\frac{\mathrm{d}\langle\underline{\boldsymbol{\sigma}}\rangle}{\mathrm{d}t}\right|_{k_t} = \left.\frac{\partial\langle\underline{\boldsymbol{\sigma}}\rangle}{\partial\langle\underline{\boldsymbol{\epsilon}}\rangle}\right|_{k_t} \left.\frac{\partial\langle\underline{\boldsymbol{\epsilon}}\rangle}{\partial t}\right|_{k_t} \tag{60}$$

Hence, the effective tangential stiffness matrix can be defined as

$${}^{k}\underline{\underline{\tilde{\mathbf{C}}}}^{*} := \left.\frac{\partial\langle\underline{\boldsymbol{\sigma}}\rangle}{\partial\langle\underline{\boldsymbol{\epsilon}}\rangle}\right|_{k_t} \tag{61}$$

The matrix $\underline{\underline{\tilde{\mathbf{C}}}}^{*}$ maps the rate of the macrostrains $\langle\dot{\underline{\boldsymbol{\epsilon}}}\rangle$ to the one of the macrostresses $\langle\dot{\underline{\boldsymbol{\sigma}}}\rangle$.

$${}^{k}\langle\dot{\underline{\boldsymbol{\sigma}}}\rangle = {}^{k}\underline{\underline{\tilde{\mathbf{C}}}}^{*k}\langle\dot{\underline{\boldsymbol{\epsilon}}}\rangle \tag{62}$$

The tangential constitutive matrix $\underline{\underline{\tilde{\mathbf{C}}}}^{*}$ can be computed analytically as will be discussed next. Since the macrostress $\langle\underline{\boldsymbol{\sigma}}\rangle$ is received as the weighted sum of the stresses $\mathbf{T}$ in Eqs. (58) and (59), the change of $\mathbf{T}$ with respect to the macrostrain $\langle\underline{\boldsymbol{\epsilon}}\rangle$ shall be computed. Therefore, the system of equation (56) needs to be differentiated with respect to the macrostrains $\langle\underline{\boldsymbol{\epsilon}}\rangle$, i.e.

$$\begin{aligned} &\mathbf{S}\frac{\partial\mathbf{T}}{\partial\langle\underline{\boldsymbol{\epsilon}}\rangle} + \mathbf{D}_u\frac{\partial\hat{\mathbf{u}}}{\partial\langle\underline{\boldsymbol{\epsilon}}\rangle} = \mathbf{K}\frac{\partial\langle\underline{\boldsymbol{\epsilon}}\rangle}{\partial\langle\underline{\boldsymbol{\epsilon}}\rangle} \\ &\mathbf{D}_T\frac{\partial\mathbf{T}}{\partial\langle\underline{\boldsymbol{\epsilon}}\rangle} - \frac{\partial\hat{\mathbf{f}}}{\partial\hat{\mathbf{u}}}\frac{\partial\hat{\mathbf{u}}}{\partial\langle\underline{\boldsymbol{\epsilon}}\rangle} = 0 \end{aligned} \tag{63}$$

Solving the upper part of Eq. (63) for $\frac{\partial\mathbf{T}}{\partial\langle\underline{\boldsymbol{\epsilon}}\rangle}$, the first equation results to

$$\frac{\partial\mathbf{T}}{\partial\langle\underline{\boldsymbol{\epsilon}}\rangle} = \mathbf{S}^{-1}\left[\mathbf{K} - \mathbf{D}_u\frac{\partial\hat{\mathbf{u}}}{\partial\langle\underline{\boldsymbol{\epsilon}}\rangle}\right] \tag{64}$$

By making use of the banded matrix $\hat{\mathbf{F}}$, defined by the gradients of the constitutive functions ${}^{(i)}\mathbf{f}^{(\beta\gamma)}$ for the interface tractions assembled in Eq. $(54)_2$:

$$\hat{\mathbf{F}} := \frac{\partial\hat{\mathbf{f}}}{\partial\mathbf{u}_s} = \mathbb{D}\begin{bmatrix} [{}^{(2)}\mathbf{f}^{(11)}\nabla_{[\![u]\!]}] & & & & & \\ & \ddots & & & & \\ & & [{}^{(2)}\mathbf{f}^{(N_\beta N_\gamma)}\nabla_{[\![u]\!]}] & & & \\ & & & [{}^{(3)}\mathbf{f}^{(11)}\nabla_{[\![u]\!]}] & & \\ & & & & \ddots & \\ & & & & & [{}^{(3)}\mathbf{f}^{(N_\beta N_\gamma)}\nabla_{[\![u]\!]}] \end{bmatrix}\mathbb{D}^{\mathrm{T}} \tag{65}$$

and introducing Eq. (64) into the lower part of (63), one obtains

$$[\mathbf{D}_T\mathbf{S}^{-1}\mathbf{D}_u + \hat{\mathbf{F}}]\frac{\partial\hat{\mathbf{u}}}{\partial\langle\underline{\boldsymbol{\epsilon}}\rangle} = \mathbf{D}_T\mathbf{S}^{-1}\mathbf{K} \tag{66}$$

The particular entries of the matrix $\hat{\mathbf{F}}$ will be given in Sections 3.1 and 3.2, where the constitutive models for the interface assumptions are introduced. The expression (66) represents a linear system of equations with six different right hand sides for the so far unknown matrix $\partial\hat{\mathbf{u}}/\partial\langle\underline{\boldsymbol{\epsilon}}\rangle$. Substituting the solution of (66) into the upper part of Eq. (63) one finds:

$$\frac{\partial\mathbf{T}}{\partial\langle\underline{\boldsymbol{\epsilon}}\rangle} = \mathbf{S}^{-1}[\mathbf{I} - \mathbf{D}_u[\mathbf{D}_T\mathbf{S}^{-1}\mathbf{D}_u + \hat{\mathbf{F}}]^{-1}\mathbf{D}_T\mathbf{S}^{-1}]\mathbf{K} \tag{67}$$

The resulting $N_T \times 6$ matrix (67) contains the partial derivatives $\partial T_{ij}/\partial\langle\epsilon_{kl}\rangle$ in the following order:

$$\frac{\partial \mathbf{T}}{\partial\langle\underline{\boldsymbol{\epsilon}}\rangle} = \begin{bmatrix} \frac{\partial T_{22}^{(1)}}{\partial\langle\epsilon_{11}\rangle} & \frac{\partial T_{22}^{(1)}}{\partial\langle\epsilon_{22}\rangle} & \frac{\partial T_{22}^{(1)}}{\partial\langle\epsilon_{33}\rangle} & \frac{\partial T_{22}^{(1)}}{\partial\langle\epsilon_{23}\rangle} & \frac{\partial T_{22}^{(1)}}{\partial\langle\epsilon_{13}\rangle} & \frac{\partial T_{22}^{(1)}}{\partial\langle\epsilon_{12}\rangle} \\ \vdots & \ddots & & & & \\ \frac{\partial T_{22}^{(N_\gamma)}}{\partial\langle\epsilon_{11}\rangle} & \frac{\partial T_{22}^{(N_\gamma)}}{\partial\langle\epsilon_{22}\rangle} & \frac{\partial T_{22}^{(N_\gamma)}}{\partial\langle\epsilon_{33}\rangle} & \frac{\partial T_{22}^{(N_\gamma)}}{\partial\langle\epsilon_{23}\rangle} & \frac{\partial T_{22}^{(N_\gamma)}}{\partial\langle\epsilon_{13}\rangle} & \frac{\partial T_{22}^{(N_\gamma)}}{\partial\langle\epsilon_{12}\rangle} \\ \frac{\partial T_{33}^{(1)}}{\partial\langle\epsilon_{11}\rangle} & \frac{\partial T_{33}^{(1)}}{\partial\langle\epsilon_{22}\rangle} & \frac{\partial T_{33}^{(1)}}{\partial\langle\epsilon_{33}\rangle} & \frac{\partial T_{33}^{(1)}}{\partial\langle\epsilon_{23}\rangle} & \frac{\partial T_{33}^{(1)}}{\partial\langle\epsilon_{13}\rangle} & \frac{\partial T_{33}^{(1)}}{\partial\langle\epsilon_{12}\rangle} \\ \vdots & \ddots & & & & \\ \frac{\partial T_{33}^{(N_\beta)}}{\partial\langle\epsilon_{11}\rangle} & \frac{\partial T_{33}^{(N_\beta)}}{\partial\langle\epsilon_{22}\rangle} & \frac{\partial T_{33}^{(N_\beta)}}{\partial\langle\epsilon_{33}\rangle} & \frac{\partial T_{33}^{(N_\beta)}}{\partial\langle\epsilon_{23}\rangle} & \frac{\partial T_{33}^{(N_\beta)}}{\partial\langle\epsilon_{13}\rangle} & \frac{\partial T_{33}^{(N_\beta)}}{\partial\langle\epsilon_{12}\rangle} \\ \frac{\partial T_{12}^{(1)}}{\partial\langle\epsilon_{11}\rangle} & \frac{\partial T_{12}^{(1)}}{\partial\langle\epsilon_{22}\rangle} & \frac{\partial T_{12}^{(1)}}{\partial\langle\epsilon_{33}\rangle} & \frac{\partial T_{12}^{(1)}}{\partial\langle\epsilon_{23}\rangle} & \frac{\partial T_{12}^{(1)}}{\partial\langle\epsilon_{13}\rangle} & \frac{\partial T_{12}^{(1)}}{\partial\langle\epsilon_{12}\rangle} \\ \vdots & \ddots & & & & \\ \frac{\partial T_{12}^{(N_\gamma)}}{\partial\langle\epsilon_{11}\rangle} & \frac{\partial T_{12}^{(N_\gamma)}}{\partial\langle\epsilon_{22}\rangle} & \frac{\partial T_{12}^{(N_\gamma)}}{\partial\langle\epsilon_{33}\rangle} & \frac{\partial T_{12}^{(N_\gamma)}}{\partial\langle\epsilon_{23}\rangle} & \frac{\partial T_{12}^{(N_\gamma)}}{\partial\langle\epsilon_{13}\rangle} & \frac{\partial T_{12}^{(N_\gamma)}}{\partial\langle\epsilon_{12}\rangle} \\ \frac{\partial T_{13}^{(1)}}{\partial\langle\epsilon_{11}\rangle} & \frac{\partial T_{13}^{(1)}}{\partial\langle\epsilon_{22}\rangle} & \frac{\partial T_{13}^{(1)}}{\partial\langle\epsilon_{33}\rangle} & \frac{\partial T_{13}^{(1)}}{\partial\langle\epsilon_{23}\rangle} & \frac{\partial T_{13}^{(1)}}{\partial\langle\epsilon_{13}\rangle} & \frac{\partial T_{13}^{(1)}}{\partial\langle\epsilon_{12}\rangle} \\ \vdots & \ddots & & & & \\ \frac{\partial T_{13}^{(N_\beta)}}{\partial\langle\epsilon_{11}\rangle} & \frac{\partial T_{13}^{(N_\beta)}}{\partial\langle\epsilon_{22}\rangle} & \frac{\partial T_{13}^{(N_\beta)}}{\partial\langle\epsilon_{33}\rangle} & \frac{\partial T_{13}^{(N_\beta)}}{\partial\langle\epsilon_{23}\rangle} & \frac{\partial T_{13}^{(N_\beta)}}{\partial\langle\epsilon_{13}\rangle} & \frac{\partial T_{13}^{(N_\beta)}}{\partial\langle\epsilon_{12}\rangle} \\ \frac{\partial T_{23}}{\partial\langle\epsilon_{11}\rangle} & \frac{\partial T_{23}}{\partial\langle\epsilon_{22}\rangle} & \frac{\partial T_{23}}{\partial\langle\epsilon_{33}\rangle} & \frac{\partial T_{23}}{\partial\langle\epsilon_{23}\rangle} & \frac{\partial T_{23}}{\partial\langle\epsilon_{13}\rangle} & \frac{\partial T_{23}}{\partial\langle\epsilon_{12}\rangle} \end{bmatrix} \tag{68}$$

It is pointed out that the terms $\partial T_{11}^{(\beta\gamma)}/\partial\langle\epsilon_{kl}\rangle$ are not given by the result (67), but can be readily computed from Eq. (36):

$$\frac{\partial T_{11}^{(\beta\gamma)}}{\partial\langle\epsilon_{kl}\rangle} = \frac{1}{\mathsf{S}_{11}^{(\beta\gamma)}} \frac{\partial\langle\epsilon_{11}\rangle}{\partial\langle\epsilon_{kl}\rangle} - \frac{\mathsf{S}_{12}^{(\beta\gamma)}}{\mathsf{S}_{11}^{(\beta\gamma)}} \frac{\partial T_{22}^{(\gamma)}}{\partial\langle\epsilon_{kl}\rangle} - \frac{\mathsf{S}_{13}^{(\beta\gamma)}}{\mathsf{S}_{11}^{(\beta\gamma)}} \frac{\partial T_{33}^{(\beta)}}{\partial\langle\epsilon_{kl}\rangle} \tag{69}$$

Hence, the elements of the stiffness matrix $\underline{\underline{\tilde{\mathbf{C}}}}^*$ follow from the stress equations (58) and (59) together with Eqs. (68) and (69):

$$\begin{aligned}
\langle\sigma_{11}\rangle &= \sum_{\gamma=1}^{N_\gamma}\sum_{\beta=1}^{N_\beta} \frac{h_\beta l_\gamma}{hl} T_{11}^{(\beta\gamma)} \rightarrow \tilde{\mathsf{C}}_{11kl}^* = \frac{\partial\langle\sigma_{11}\rangle}{\partial\langle\epsilon_{kl}\rangle} = \sum_{\gamma=1}^{N_\gamma}\sum_{\beta=1}^{N_\beta} \frac{h_\beta l_\gamma}{hl} \frac{\partial T_{11}^{(\beta\gamma)}}{\partial\langle\epsilon_{kl}\rangle} \\
\langle\sigma_{22}\rangle &= \sum_{\gamma=1}^{N_\gamma} \frac{l_\gamma}{l} T_{22}^{(\gamma)} \rightarrow \tilde{\mathsf{C}}_{22kl}^* = \frac{\partial\langle\sigma_{22}\rangle}{\partial\langle\epsilon_{kl}\rangle} = \sum_{\gamma=1}^{N_\gamma} \frac{l_\gamma}{l} \frac{\partial T_{22}^{(\gamma)}}{\partial\langle\epsilon_{kl}\rangle} \\
\langle\sigma_{33}\rangle &= \sum_{\beta=1}^{N_\beta} \frac{h_\beta}{h} T_{33}^{(\beta)} \rightarrow \tilde{\mathsf{C}}_{33kl}^* = \frac{\partial\langle\sigma_{33}\rangle}{\partial\langle\epsilon_{kl}\rangle} = \sum_{\beta=1}^{N_\beta} \frac{h_\beta}{h} \frac{\partial T_{33}^{(\beta)}}{\partial\langle\epsilon_{kl}\rangle} \\
\langle\sigma_{23}\rangle &= T_{23} \rightarrow \tilde{\mathsf{C}}_{23kl}^* = \frac{\partial\langle\sigma_{23}\rangle}{\partial\langle\epsilon_{kl}\rangle} = \sum_{\gamma=1}^{N_\gamma}\sum_{\beta=1}^{N_\beta} \frac{h_\beta l_\gamma}{hl} \frac{\partial T_{23}}{\partial\langle\epsilon_{kl}\rangle} \\
\langle\sigma_{31}\rangle &= \sum_{\beta=1}^{N_\beta} \frac{h_\beta}{h} T_{31}^{(\beta)} \rightarrow \tilde{\mathsf{C}}_{31kl}^* = \frac{\partial\langle\sigma_{31}\rangle}{\partial\langle\epsilon_{kl}\rangle} = \sum_{\beta=1}^{N_\beta} \frac{h_\beta}{h} \frac{\partial T_{31}^{(\beta)}}{\partial\langle\epsilon_{kl}\rangle} \\
\langle\sigma_{21}\rangle &= \sum_{\gamma=1}^{N_\gamma} \frac{l_\gamma}{l} T_{21}^{(\gamma)} \rightarrow \tilde{\mathsf{C}}_{21kl}^* = \frac{\partial\langle\sigma_{21}\rangle}{\partial\langle\epsilon_{kl}\rangle} = \sum_{\gamma=1}^{N_\gamma} \frac{l_\gamma}{l} \frac{\partial T_{21}^{(\gamma)}}{\partial\langle\epsilon_{kl}\rangle}
\end{aligned} \tag{70}$$

The tangential stiffness terms in Eqs. (70) are assembled to the matrix $\underline{\underline{\tilde{\mathbf{C}}}}^{*}$ in the following form:

$$[\tilde{C}_{ij}] = \begin{bmatrix} \tilde{C}^{*}_{1111} & \tilde{C}^{*}_{1122} & \tilde{C}^{*}_{1133} & \tilde{C}^{*}_{1123} & \tilde{C}^{*}_{1131} & \tilde{C}^{*}_{1121} \\ \tilde{C}^{*}_{2211} & \tilde{C}^{*}_{2222} & \tilde{C}^{*}_{2233} & \tilde{C}^{*}_{2223} & \tilde{C}^{*}_{2231} & \tilde{C}^{*}_{2221} \\ \tilde{C}^{*}_{3311} & \tilde{C}^{*}_{3322} & \tilde{C}^{*}_{3333} & \tilde{C}^{*}_{3323} & \tilde{C}^{*}_{3331} & \tilde{C}^{*}_{3321} \\ \tilde{C}^{*}_{2311} & \tilde{C}^{*}_{2322} & \tilde{C}^{*}_{2333} & \tilde{C}^{*}_{2323} & \tilde{C}^{*}_{2331} & \tilde{C}^{*}_{2321} \\ \tilde{C}^{*}_{3111} & \tilde{C}^{*}_{3122} & \tilde{C}^{*}_{3133} & \tilde{C}^{*}_{3123} & \tilde{C}^{*}_{3131} & \tilde{C}^{*}_{3121} \\ \tilde{C}^{*}_{2111} & \tilde{C}^{*}_{2122} & \tilde{C}^{*}_{2133} & \tilde{C}^{*}_{2123} & \tilde{C}^{*}_{2131} & \tilde{C}^{*}_{2121} \end{bmatrix} \tag{71}$$

Eq. (71) represents the matrix notation of the constitutive tensor $\tilde{\mathbb{C}}^{*}$ which is defined on the right of Eq. (7) and hence depends implicitly on the tangential strain concentration tensors $\tilde{\mathbb{A}}^{(i)}$ of the phases i. It is emphasised that the matrix $\underline{\underline{\tilde{\mathbf{C}}}}^{*}$ is fully occupied by non-zero elements for general strain processes $\langle \underline{\underline{\boldsymbol{\epsilon}}} \rangle$. This is due to the coupling of the normal and shear stiffnesses of the interface models described in the following Section 3. The immanent lack of normal-shear-coupling, which is characteristic for the GMC-model, is herewith not cancelled: pure shear strain processes still only raise shear stress responses and pure normal strain processes result to normal stresses only. But for combined loading histories, the evolution of the normal macrostress responses is affected by the macroshear strains and vice versa as long as the damage evolves in the flexible interfaces (i.e. $\dot{q} > 0$). This two way interference is caused by the coupling of the normal and shear interface stiffnesses, depending explicitly on the damage variable q, which is itself a functional of the history of both the normal and the tangential displacement discontinuities.

3. Interface models

As mentioned in the introduction a variety of interface models is available. In this section the models of Chaboche et al. (1997) and Lissenden (1996) will be discussed in detail. The latter model is simular to the one of Chaboche but comes without any initial compliance of the interface before softening of the bond takes place, see Fig. 3. Hence, it is not only recommended to model perfect fibre–matrix-bonding but also to account for the development of matrix cracks at the intrinsic inner surfaces along the subcell boundaries of the GMC-Model as well. Lissenden (1999) already implemented the interface model given below into the original GMC for metal matrix composites. In this paper a more rigorous portray of Lissendens model is given. An evolving internal variable is introduced as a functional of the loading history. This is an important feature if cyclic loading processes are to be considered. The linearization of the two interface models are given for loading and unloading paths, since they are needed for the iterative solution of the nonlinear GMC-model as wells as for the computation of the tangential stiffness matrix.

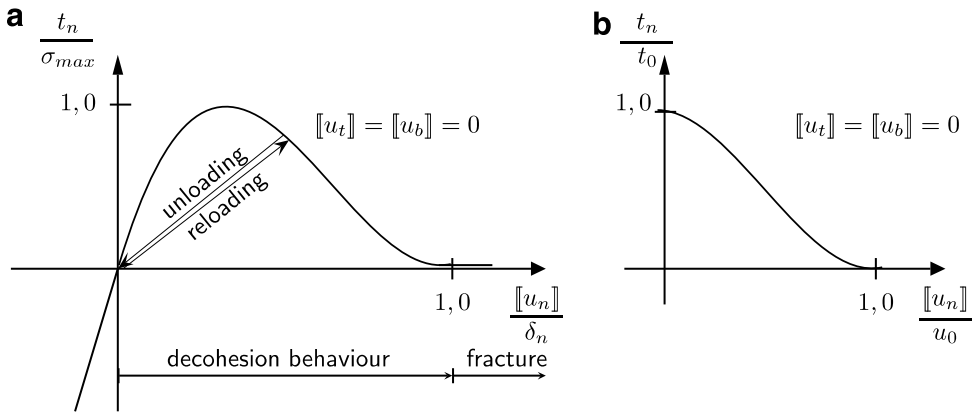

Fig. 3. Normalised tractions under pure mode I conditions versus normalised interface separation: (a) model of Chaboche with initial interface compliance, (b) model of Lissenden without initial interface compliance before debonding.

3.1. Interface model with initial compliance

The displacement jumps are pruned of their dimension by dividing them by some characteristic length parameters δ_n, δ_t and δ_b, respectively. Based on the normalised displacement jumps, a history function over past times $\tau \in [-\infty, t]$ is introduced in terms of the weighted norm defined as follows:

$$\|\mathbf{u}(\tau)\| = \sqrt{\left(\frac{\max\{0, [\![u_n(\tau)]\!]\}}{\delta_n}\right)^2 + \left(\frac{[\![u_t(\tau)]\!]}{\delta_t}\right)^2 + \left(\frac{[\![u_b(\tau)]\!]}{\delta_b}\right)^2} \tag{72}$$

The term $\max\{0, [\![u_n(\tau)]\!]\}$ states that only the positive normal component $[\![u_n]\!]$ for tension contributes to the norm, that is

$$\max\{0, [\![u_n]\!]\} = \begin{cases} [\![u_n]\!], & [\![u_n]\!] > 0 \\ 0, & [\![u_n]\!] \leqslant 0 \end{cases} \tag{73}$$

By this restriction a compressive normal traction does not expedite any damage propagation. Because of the history dependence the damage variable $q \in [0,1]$ is defined by means of the history functional of the past deformation process in order to describe irreversible damage due to debonding or cracking:

$$q(t) = \mathscr{F}(\mathbf{u}(\tau))_{\tau \geqslant -\infty}^{\tau = t} := \min\left\{\max_{\tau \leqslant t} \|\mathbf{u}(\tau)\|, 1\right\} \tag{74}$$

By its definition the internal variable q measures and stores the maximum displacement discontinuity that has ever occurred during past times $\tau \leqslant t$, see Fig. 4. The value $q = 0$ stands for the undamaged initial configuration. If q approaches 1, total fracture of the bond between the phases occurs. Thus, q is monotonously increasing and bounded above.

The maximum of the achieveable normal traction t_n under pure mode I conditions is denoted by $\sigma_{\max}$: see Fig. 3a. Similarly, under pure mode II or III conditions the maximum of the tangential tractions t_t or t_b is denoted by $\tau_{\max}$. The ratio of the shear-to-normal strength is expressed by $\alpha = \tau_{\max}/\sigma_{\max}$. The actual traction vector $\mathbf{t}$ is given by the function $\mathbf{f}(\mathbf{u}, q)$:

$$\mathbf{t} = \mathbf{f}(\mathbf{u}, q) = \begin{Bmatrix} f_n(\mathbf{u}, q) \\ f_t(\mathbf{u}, q) \\ f_b(\mathbf{u}, q) \end{Bmatrix} = F(q) \begin{Bmatrix} \frac{[\![u_n]\!]}{\delta_n} \\ \alpha \frac{[\![u_t]\!]}{\delta_t} \\ \alpha \frac{[\![u_b]\!]}{\delta b} \end{Bmatrix} \tag{75}$$

The term $F(q)$, which depends explicitly on the damage variable q, is defined as

$$F(q) = \frac{27}{4}\sigma_{\max}(1-q)^2 \tag{76}$$

The factor 27/4 in Eq. (76) ensures that in the case of pure mode I conditions the normalised cubic traction-separation-function $f_n(\mathbf{u}, q)/\sigma_{\max}$ – see Fig. 3a – possesses the maximum value 1 as well as a horizontal tangent for the normalised displacement $u_n/\delta_n = 1$. The term $F(q)$ can be interpreted as the secant stiffness of the

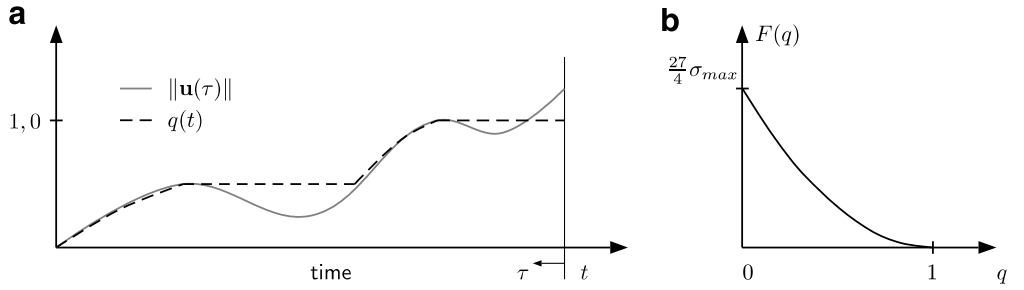

Fig. 4. (a) Evolution of the damage variable q over past times $\tau \leqslant t$ depending on the history function $\|\mathbf{u}(\tau)\|$. (b) Interface stiffness function $F(q)$.

interface model. In the case of a monotonous initial loading of the interface, the stiffness $F(q)$ depends implicitly on the current interface discontinuity vector $\mathbf{u}$, because $q(t)$ equals $\|\mathbf{u}(t)\|$ according to Eq. (74), see Fig. 4a. During unloading the scalar q is fixed and the stiffness $F(q)$ is kept constant. In the case of compression on the interface the phases may not undergo an unrealistic interpenetration. Therefore, Chaboche et al. (1997) suggests to set the stiffness modulus K of the interface material to a reasonable high numerical value. The constitutive expression for the normal traction t_n of Eq. (75) is replaced by

$$f_n(\mathbf{u},q)=\begin{cases} K\frac{[\![u_n]\!]}{\delta_n} & \forall q \text{ if } t_n<0 \\ F(q)\frac{[\![u_n]\!]}{\delta_n} & \forall q \text{ if } t_n\geqslant 0 \end{cases} \tag{77}$$

Since the gradient of the traction function $\mathbf{f}$ is needed for the iterative solution of Eqs. (56) as well as for the matrix $\hat{\mathbf{F}}$ according to Eq. (65), it will be derived here for it was not given by Chaboche et al. (1997) explicitly. Defining the nabla operator as

$$\nabla_{[\![\mathbf{u}]\!]}:=\left\{\frac{\partial}{\partial[\![u_n]\!]}\quad\frac{\partial}{\partial[\![u_t]\!]}\quad\frac{\partial}{\partial[\![u_b]\!]}\right\} \tag{78}$$

and applying it to the constitutive function $\mathbf{f}$ in Eq. (75) for the traction vector $\mathbf{t}$, the matrix notation of the gradient $\mathbf{f}\otimes\nabla_{[\![u]\!]}$ for combined tension and shear is given as

$$\mathbf{f}\nabla_{[\![u]\!]}=\begin{bmatrix} \frac{\partial F(q)}{\partial[\![u_n]\!]}\frac{[\![u_n]\!]}{\delta_n}+\frac{F(q)}{\delta_n} & \frac{\partial F(q)}{\partial[\![u_t]\!]}\frac{[\![u_n]\!]}{\delta_n} & \frac{\partial F(q)}{\partial[\![u_b]\!]}\frac{[\![u_n]\!]}{\delta_n} \\ \alpha\frac{\partial F(q)}{\partial[\![u_n]\!]}\frac{[\![u_t]\!]}{\delta_t} & \alpha\left(\frac{\partial F(q)}{\partial[\![u_t]\!]}\frac{[\![u_t]\!]}{\delta_t}+\frac{F(q)}{\delta_t}\right) & \alpha\frac{\partial F(q)}{\partial[\![u_b]\!]}\frac{[\![u_t]\!]}{\delta_t} \\ \alpha\frac{\partial F(q)}{\partial[\![u_n]\!]}\frac{[\![u_b]\!]}{\delta_b} & \alpha\frac{\partial F(q)}{\partial[\![u_t]\!]}\frac{[\![u_b]\!]}{\delta_b} & \alpha\left(\frac{\partial F(q)}{\partial[\![u_b]\!]}\frac{[\![u_b]\!]}{\delta_b}+\frac{F(q)}{\delta_b}\right) \end{bmatrix} \tag{79}$$

and in case of interface compression and shear:

$$\mathbf{f}\nabla_{[\![u]\!]}=\begin{bmatrix} \frac{K}{\delta_n} & 0 & 0 \\ 0 & \alpha\left(\frac{\partial F(q)}{\partial[\![u_t]\!]}\frac{[\![u_t]\!]}{\delta_t}+\frac{F(q)}{\delta_t}\right) & \alpha\frac{\partial F(q)}{\partial[\![u_b]\!]}\frac{[\![u_t]\!]}{\delta_t} \\ 0 & \alpha\frac{\partial F(q)}{\partial[\![u_t]\!]}\frac{[\![u_b]\!]}{\delta_b} & \alpha\left(\frac{\partial F(q)}{\partial[\![u_b]\!]}\frac{[\![u_b]\!]}{\delta_b}+\frac{F(q)}{\delta_b}\right) \end{bmatrix} \tag{80}$$

The interface function $F(q)$ depends implicitly on the displacement jumps and is derivated with respect to the components of the displacement discontinuity vector at current time t by means of the chain rule:

$$\begin{aligned} \left.\frac{\partial F}{\partial[\![u_n]\!]}\right|_t &= \left.\frac{\partial F}{\partial q}\frac{\partial q}{\partial\|\mathbf{u}\|}\frac{\partial\|\mathbf{u}\|}{\partial[\![u_n]\!]}\right|_t \\ \left.\frac{\partial F}{\partial[\![u_t]\!]}\right|_t &= \left.\frac{\partial F}{\partial q}\frac{\partial q}{\partial\|\mathbf{u}\|}\frac{\partial\|\mathbf{u}\|}{\partial[\![u_t]\!]}\right|_t \\ \left.\frac{\partial F}{\partial[\![u_b]\!]}\right|_t &= \left.\frac{\partial F}{\partial q}\frac{\partial q}{\partial\|\mathbf{u}\|}\frac{\partial\|\mathbf{u}\|}{\partial[\![u_b]\!]}\right|_t \end{aligned} \tag{81}$$

The first two partial derivatives, appearing on the right sides of Eqs. (81), read as follows:

$$\left.\frac{\partial F}{\partial q}\right|_t=-\frac{27}{2}\sigma_{\max}(1-q) \tag{82}$$

$$\left.\frac{\partial q}{\partial\|\mathbf{u}\|}\right|_t=\frac{\partial q(t)}{\partial\|\mathbf{u}(t)\|}=\begin{cases} 1 & \text{if } q(t)=\|\mathbf{u}\|(t) \text{ (first loading)} \\ 0 & \text{else (unloading or reloading)} \end{cases} \tag{83}$$

Due to Eq. (74) the stiffness function $F(q)$ degrades with the actual displacement jumps only in the case of first loading – see Fig. 4(a) and Eq. $(83)_1$ – otherwise it remains constant as given by Eqs. $(83)_2$ and (82). During

unloading or reloading processes the matrices (79) or (80) only possess constant none zero entries $F(q)/\delta_n$ and $F(q)/\delta_t$ on their main diagonals. Hence, the unloading and reloading paths follow a secant to the stress–displacement-curve as depicted by Fig. 3(a). The partial derivatives of the norm of the discontinuity vector $\|\mathbf{u}\|$ in terms of the components are given by

$$\left.\frac{\partial\|\mathbf{u}\|}{\partial[\![u_n]\!]}\right|_t = \frac{\max\{0,[\![u_n]\!]\}}{\delta_n^2\sqrt{\left(\frac{\max\{0,[\![u_n]\!]\}}{\delta_n}\right)^2+\left(\frac{[\![u_t]\!]}{\delta_t}\right)^2+\left(\frac{[\![u_b]\!]}{\delta_b}\right)^2}} = \frac{\langle[\![u_n]\!]\rangle}{\delta_n^2\|\mathbf{u}\|(t)} \tag{84}$$

$$\left.\frac{\partial\|\mathbf{u}\|}{\partial[\![u_t]\!]}\right|_t = \frac{[\![u_t]\!]}{\delta_t^2\sqrt{\left(\frac{\max\{0,[\![u_n]\!]\}}{\delta_n}\right)^2+\left(\frac{[\![u_t]\!]}{\delta_t}\right)^2+\left(\frac{[\![u_b]\!]}{\delta_b}\right)^2}} = \frac{[\![u_t]\!]}{\delta_t^2\|\mathbf{u}\|(t)} \tag{85}$$

$$\left.\frac{\partial\|\mathbf{u}\|}{\partial[\![u_b]\!]}\right|_t = \frac{[\![u_b]\!]}{\delta_b^2\sqrt{\left(\frac{\max\{0,[\![u_n]\!]\}}{\delta_n}\right)^2+\left(\frac{[\![u_t]\!]}{\delta_t}\right)^2+\left(\frac{[\![u_b]\!]}{\delta_b}\right)^2}} = \frac{[\![u_b]\!]}{\delta_b^2\|\mathbf{u}\|(t)} \tag{86}$$

where $\langle\,\rangle$ is the MACAULY bracket in Eq. (84).

3.2. Interface model with initial infinite stiffness

The interface model given by Lissenden (1996) introduces the ductility parameters u_0 for the normal direction and ζu_0 for the two tangential directions to define the time varying scalar function $\|\mathbf{u}(\tau)\|$ with $-\infty \leqslant \tau \leqslant t$ of the normalised components of the displacement discontinuity vector:

$$\|\mathbf{u}\|(\tau)\| := \sqrt{\left(\frac{\max\{0,[\![u_n]\!](\tau)\}}{u_0}\right)^2+\left(\frac{[\![u_t]\!](\tau)}{\zeta u_0}\right)^2+\left(\frac{[\![u_b]\!](\tau)}{\zeta u_0}\right)^2} \tag{87}$$

The parameter ζ is called the tangential-to-normal ductility ratio. The normal strength is denoted by t_0 and the tangential strength is given as ηt_0 with the shear-to-normal strength ratio η. The quadratic interaction criterion of the normalised interface tractions

$$t_v := \sqrt{\left(\frac{\max\{0,t_n\}}{t_0}\right)^2+\left(\frac{t_t}{\eta t_0}\right)^2+\left(\frac{t_b}{\eta t_0}\right)^2} \tag{88}$$

is defined to predict the initiation of debonding or crack evolution. As long as $t_v < 1$ the displacement field is continuous across the interfaces. Once t_v has been equal to one, the interfacial traction vector reaches its maximal strength and degrades afterwards during first loading with the monotonously increasing displacement discontinuities as follows:

$$\mathbf{t} = \mathbf{f}(\mathbf{u},q) = \begin{Bmatrix} f_n(\mathbf{u},q) \\ f_t(\mathbf{u},q) \\ f_b(\mathbf{u},q) \end{Bmatrix} = \frac{t_0}{u_0}F(q)\begin{Bmatrix} [\![u_n]\!] \\ \frac{\eta}{\zeta}[\![u_t]\!] \\ \frac{\eta}{\zeta}[\![u_b]\!] \end{Bmatrix} \tag{89}$$

Herein, the term $F(q)$ may be interpreted as a dimensionless stiffness of the interface. It is assumed to be

$$F(q) = \frac{1-3q^2+2q^3}{q} \tag{90}$$

and to depend on the damage variable $q \in [0,1]$, which is defined as in Eq. (74) on the basis of Eq. (87) for $\|\mathbf{u}(\tau)\|$ as

$$q(t) = \mathscr{F}(\mathbf{u})_{\tau\geqslant-\infty}^{\tau=t} := \min\left\{\max_{\tau\leqslant t}\|\mathbf{u}(\tau)\|, 1\right\} \tag{91}$$

In the case of a compressive loading, the interpenetration of the phases is prevented by completing the constitutive assumption for the normal component of the traction vector in Eq. (89) by the expression $t_n = K\frac{[\![u_n]\!]}{u_0}$,

where the stiffness modulus K of the interface is set to a reasonable but sufficiently high value. By applying the nabla operator of Eq. (78) to the traction function $\mathbf{f}$ of Eq. (89) the matrix notation of the gradient $\mathbf{f} \otimes \nabla_{[\![u]\!]}$ becomes in the case of combined tension and shear:

$$\mathbf{f}\nabla_{[\![u]\!]} = \frac{t_0}{u_0}\begin{bmatrix} \dfrac{\partial F(q)}{\partial [\![u_n]\!]}[\![u_n]\!] + F(q) & \dfrac{\partial F(q)}{\partial [\![u_t]\!]}[\![u_n]\!] & \dfrac{\partial F(q)}{\partial [\![u_b]\!]}[\![u_b]\!] \\ \dfrac{\eta}{\zeta}\dfrac{\partial F(q)}{\partial [\![u_n]\!]}[\![u_t]\!] & \dfrac{\eta}{\zeta}\left(\dfrac{\partial F(q)}{\partial [\![u_t]\!]}[\![u_t]\!] + F(q)\right) & \dfrac{\eta}{\zeta}\dfrac{\partial F(q)}{\partial [\![u_b]\!]}[\![u_t]\!] \\ \dfrac{\eta}{\zeta}\dfrac{\partial F(q)}{\partial [\![u_n]\!]}[\![u_b]\!] & \dfrac{\eta}{\zeta}\dfrac{\partial F(q)}{\partial [\![u_t]\!]}[\![u_b]\!] & \dfrac{\eta}{\zeta}\left(\dfrac{\partial F(q)}{\partial [\![u_b]\!]}[\![u_b]\!] + F(q)\right) \end{bmatrix} \tag{92}$$

and for combined compression and shear:

$$\mathbf{f}\nabla_{[\![u]\!]} = \frac{t_0}{u_0}\begin{bmatrix} \dfrac{K}{t_0} & 0 & 0 \\ 0 & \dfrac{\eta}{\zeta}\left(\dfrac{\partial F(q)}{\partial [\![u_t]\!]}[\![u_t]\!] + F(q)\right) & \dfrac{\eta}{\zeta}\dfrac{\partial F(q)}{\partial [\![u_b]\!]}[\![u_t]\!] \\ 0 & \dfrac{\eta}{\zeta}\dfrac{\partial F(q)}{\partial [\![u_t]\!]}[\![u_b]\!] & \dfrac{\eta}{\zeta}\left(\dfrac{\partial F(q)}{\partial [\![u_b]\!]}[\![u_b]\!] + F(q)\right) \end{bmatrix} \tag{93}$$

The partial derivatives, emerging from Eqs. (92) and (93)

$$\left.\frac{\partial F(q)}{\partial [\![u_i]\!]}\right|_t = \frac{\partial F}{\partial q}\frac{\partial q}{\partial \|\mathbf{u}\|}\left.\frac{\partial \|\mathbf{u}\|}{\partial [\![u_i]\!]}\right|_t, \quad i = n,t,b \tag{94}$$

are computed from the following expressions:

$$\begin{aligned} \left.\frac{\partial F}{\partial q}\right|_t &= \frac{4q^3 - 3q^2 - 1}{q^2} \\ \left.\frac{\partial q}{\partial \|\mathbf{u}\|}\right|_t &= \frac{\partial q(t)}{\partial \|\mathbf{u}(t)\|} = \begin{cases} 1 & \text{if } q(t) = \|\mathbf{u}\|(t) \text{ (first loading)} \\ 0 & \text{else (unloading or reloading)} \end{cases} \\ \left.\frac{\partial \|\mathbf{u}\|}{\partial [\![u_n]\!]}\right|_t &= \frac{\langle [\![u_n]\!] \rangle}{u_0^2 \|\mathbf{u}\|(t)} \\ \left.\frac{\partial \|\mathbf{u}\|}{\partial [\![u_t]\!]}\right|_t &= \frac{[\![u_t]\!]}{\zeta^2 u_0^2 \|\mathbf{u}\|(t)} \\ \left.\frac{\partial \|\mathbf{u}\|}{\partial [\![u_b]\!]}\right|_t &= \frac{[\![u_b]\!]}{\zeta^2 u_0^2 \|\mathbf{u}\|(t)} \end{aligned} \tag{95}$$

4. Numerical results

The current paper only presents parametric studies in order to solely investigate the influence of the interface parameters on the overall stress responses qualitatively. Since it is well known that some resin materials show nonlinearly elastic behaviour in shear – see e.g. Hahn and Tsai (1973) – it is intended to enhance the GMC-model by first implementing a nonlinear-elastic constitutive model for the matrix cells before the interface parameters are identified. The important latter task is postponed to a forthcoming paper that will dedicate to the validation of the enhanced GMC-Model using the experimental data of the so called *World Wide Failure Exercise* – see Soden and Hinton (1998)

In the following a unidirectionally reinforced resin with glass fibres is investigated as a composite material. Both material phases, utilised for the subsequent numerical analyses, are assumed to behave linearly elastic and isotropic. The epoxy matrix material is characterised by its shear modulus $G_m = 1.3$ GPa and bulk modulus $K_m = 3.8$ GPa. The reinforcing glass fibres possess a diameter of $d_f = 6$ μm. Its shear modulus is assumed to $G_f = 34.0$ GPa and its bulk modulus to $K_f = 46.6$ GPa. The volume fraction $c_f = 0.45$ of the fibres remains

unchanged. The ratios α and η of shear-to-normal strength as well as the tangential-to-normal ratios δ_n/δ_t and ζ of the ductility of the interfaces are chosen to be equal to one for both interface models. The absolute values of the interface strengths $\sigma_{\max}$ and t_n and the ductility parameters u_0 and δ_n are altered. It is well known from experimental testings of fibre reinforced epoxy materials that the onset of fibre/matrix debonding is usually accompanied by the brittle damage of the matrix phase. Despite of this the first numerical examples only consider the debonding of the fibres from the matrix as the solely present damage process. For the lack of given interface parameters in the literature, the influence of the bond model parameters on the average responses is studied qualitatively. Hence, it is desirable to avoid at first the interference of debonding with matrix damage effects. The additional appearance of discrete cracks within the matrix phase will be considered in Section 4.2.

4.1. Fibre debonding

Fibre debonding from the matrix is studied first, where the matrix material is assumed to behave linearly elastically. It is well known that matrix cracking occurs in the wake of fibre debonding in glass fibre reinforced epoxy resins. However, only fibre debonding is considered in this section in order to verify the failure algorithm and to gain confidence in the GMC-model with damage. Figs. 5 and 6 illustrate the evolution of the

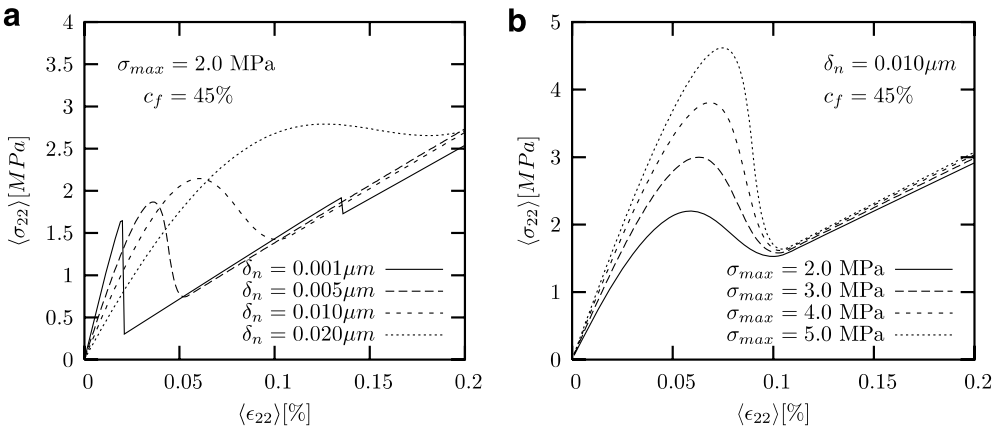

Fig. 5. Comparison of the stress responses $\langle\sigma_{22}\rangle$ to the monotonically increased strain $\langle\epsilon_{22}\rangle$ based on the Chaboche interface model. (a) Variation of length parameter δ_n keeping the bond strength $\sigma_{\max}$ constant. (b) Variation of the bond strength $\sigma_{\max}$ for a constant length parameter δ_n.

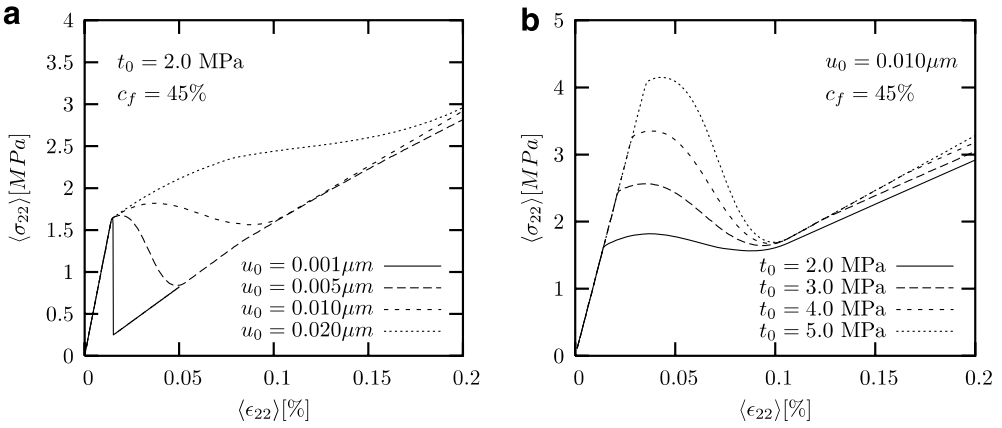

Fig. 6. Comparison of the stress responses $\langle\sigma_{22}\rangle$ to the monotonically increased strain $\langle\epsilon_{22}\rangle$ based on the Lissenden interface model. (a) Variation of length parameters u_0 keeping the bond strength t_0 constant. (b) Variation of the bond strengths t_0 for a constant length parameter u_0.

macrostress $\langle\sigma_{22}\rangle$ computed from the four cells model with two fibre–matrix interfaces subjected to a monotonically increasing macrostrain $\langle\epsilon_{22}\rangle$. All other strain components are equal to zero. The results of Fig. 5(a) and (b) are obtained from the Chaboche model, whereas Fig. 6(a) and (b) shows the corresponding results of the Lissenden model. The steep slope of the stress $\langle\sigma_{22}\rangle$-strain-curve is followed by a slow increase of the stress after debonding of the fibre has occurred. The stress–strain-curves in Figs. 5(a) and 6(a) become smoother with an increasing ductility δ_n or u_0 of the interface. The overall behaviour is less brittle. The level of the average stress $\langle\sigma_{22}\rangle$ that is achieved prior to the total debonding rises and the local stress maximum shifts to a higher macroscopic strain. The increase of the bond strength mainly intensifies the hump of the stress–strain-curve, see Figs. 5(b) and 6(b). The macroscopic stress responses $\langle\sigma_{21}\rangle$ of the unit cell, undergoing a simple shear deformation process $\langle\epsilon_{21}\rangle > 0$, are given by Fig. 7 for the interface model of Chaboche. The stress responses $\langle\sigma_{21}\rangle$ in Fig. 8 are received by applying the Lissenden model. The stress–strain-curves, illustrated in Figs. 7 and 8, are qualitatively similar to those belonging to the normal strain process $\langle\epsilon_{22}\rangle$. The perceptible difference is that all curves are joining a common straight line after having surpassed the local stress maximum. This phenomenon is due to the fact that only the interface perpendicular to the x_2-axis is affected by shear

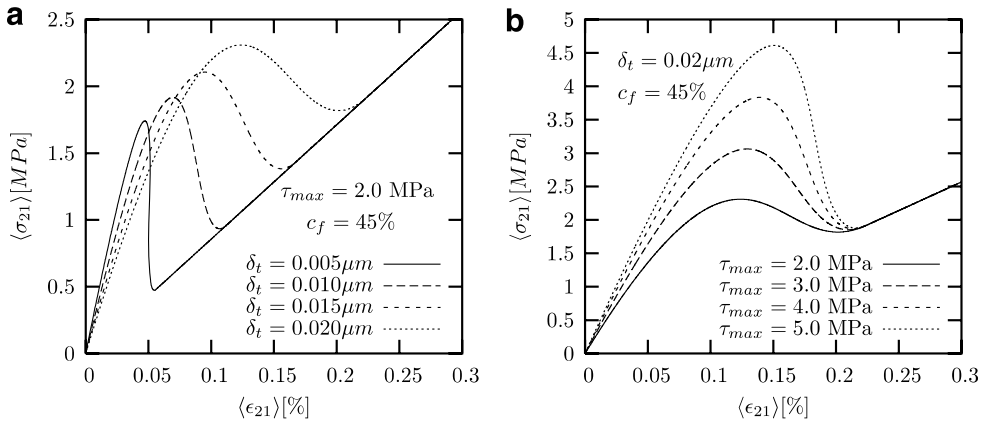

Fig. 7. Comparison of the stress responses $\langle\sigma_{21}\rangle$ to the monotonically increased strain $\langle\epsilon_{21}\rangle$ based on the Chaboche interface model. (a) Variation of the length parameter δ_t keeping the bond strength $\tau_{\max}$ constant. (b) Variation of the bond strength $\tau_{\max}$ for a constant length parameter δ_t.

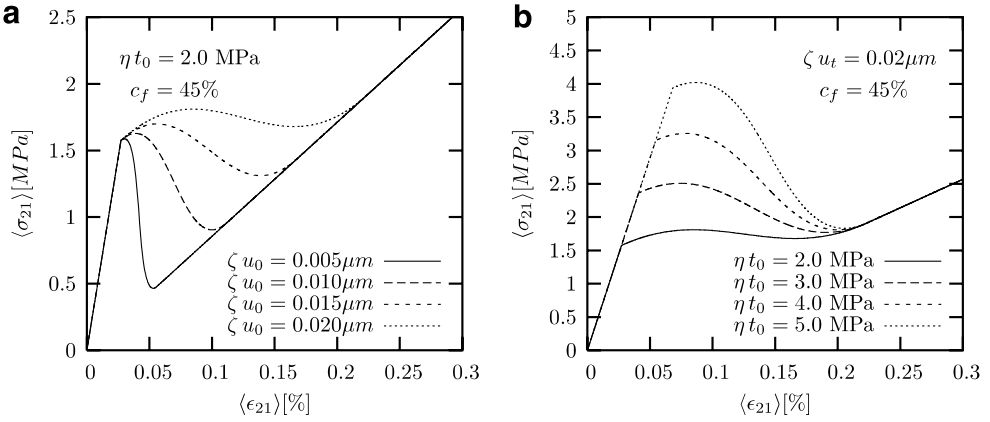

Fig. 8. Comparison of the stress responses $\langle\sigma_{21}\rangle$ to the monotonically increased strain $\langle\epsilon_{21}\rangle$ based on the Lissenden interface model. (a) Variation of the length parameter ζu_0 keeping the bond strength ηt_0 constant. (b) Variation of the bond strength ηt_0 for a constant length parameter ζu_0.

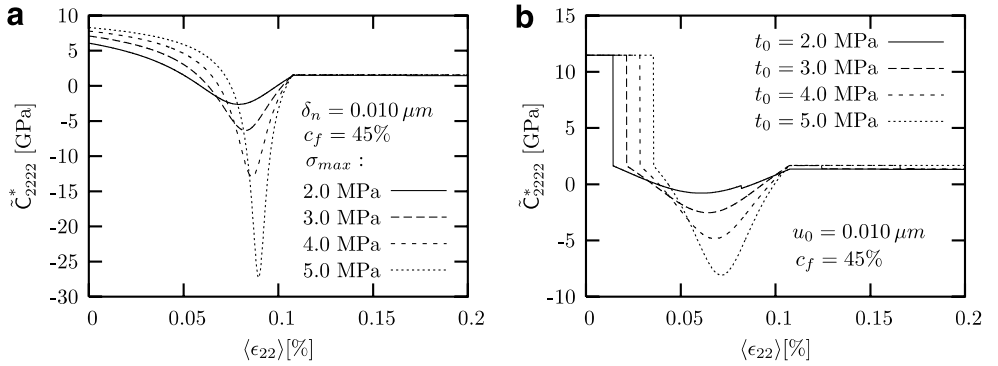

Fig. 9. Tangential stiffness component $\tilde{C}^*_{2222}$ vs. $\langle\epsilon_{22}\rangle$: (a) Chaboche and (b) Lissenden.

deformations $\langle\epsilon_{21}\rangle$ in contrast to the normal strain process $\langle\epsilon_{22}\rangle > 0$, where (σ_{33}) is non-zero and causes the damage of the interface perpendicular to the x_3-axis as well. Thus, the second and smaller softening response in the stress–strain-curve, given by Fig. 5(a) for $\delta_n = 0.001$ μm, is caused by the brittle fracture of the second interface. As a consequence of the initial interface compliance, appearing in the model of Chaboche, the initial tangential stiffness components $\tilde{C}^*_{ijkl}$ of Eq. (8) depend on the particular choice of the interface parameters, see Fig. 9. This effect does not occur by using the Lissenden model. Thus, the initial macroscopic stiffnesses are considerably higher and constantly equal to those of a composite with perfectly bonded phases until the debonding process is initiated.

4.2. Matrix cracking and fibre debonding

The GMC offers two alternatives in order to model realistically the damage of the composite, i.e. the softening and the total fracture of the matrix material besides the fibre debonding, due to the growth of microcracks from the interface into the matrix. The first one would be to degrade the elastic moduli for each matrix subcell individually as a function of the subcell strains. The second approach, which is applied here, uses the intrinsic inner surfaces of the GMC-discretisation as localisation nuclei for the formation of macro-cracks. Thus, the behaviour of the assumed cracks will be controlled by an appropriate interface formulation, as it is given by the model of Lissenden. Obviously, the usage of the model of Chaboche with its initial compliance is not recommendable in this context. In the following simulations the influence of the strength and ductility parameters on the model responses is studied. The behaviour of the matrix–matrix interfaces (MM-interfaces) are described by the Lissenden model exclusively, whereas the debonding of the fibre/matrix interfaces (FM-interfaces) is modelled by the approaches of Lissenden or Chaboche. The calculations are carried out for the model with four cells and two FM- and MM-interfaces. Fig. 10(a) shows the stress response $\langle\sigma_{22}\rangle$ versus the prescribed strain $\langle\epsilon_{22}\rangle$ of the Lissenden model used for both the FM- and the MM-interfaces. Up to the point where the interface traction t_n of the MM-interface perpendicular to the x_2-direction reaches its maximum value $t_0|_{\mathrm{MM}}$, all stress–strain-curves coincide exactly with the one of the linear elastic matrix material. Beyond that point, the stress responses diverge from each other. The degree of softening depends on the ductility parameter. The smaller $u_0|_{\mathrm{MM}}$ is chosen, the more brittle turns out to be the failure of the matrix phase. The stress responses, given in Fig. 10(b), are obtained by keeping the ductility parameter constant $u_0|_{\mathrm{MM}} = 0.015$ μm but increasing the strength parameter $t_0|_{\mathrm{MM}}$ only. As expected, the macroscopic strength of the composite material also increases. If the ductility $u_0|_{\mathrm{MM}}$ is kept constant, the total fracture of the composite takes place at the same strain level which is not altered by varying the strength parameter $t_0|_{\mathrm{MM}}$.

Fig. 11(a) and (b) illustrate the course of macroscopic responses $\langle\sigma_{22}\rangle$ versus the macroscopic strain $\langle\epsilon_{22}\rangle$ if the Chaboche model for the FM- and the Lissenden model for the MM-interfaces is applied. Again the ductility and strength parameters of the MM-interfaces are varied. Their effects on the overall response are the same as in the case described above.

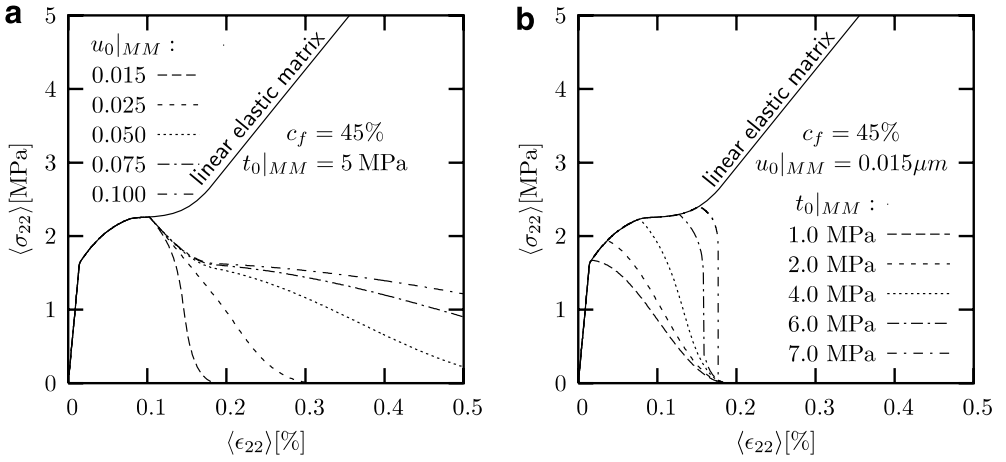

Fig. 10. Stress–strain-curves with matrix cracking. FM-Interfaces: $t_0|_{\mathrm{FM}} = 2$ MPa, $u_0|_{\mathrm{FM}} = 0.015$ μm. (a) Variation of MM-interface parameter $u_0|_{\mathrm{MM}}$. (b) Variation of MM-interface parameter $t_0|_{\mathrm{MM}}$.

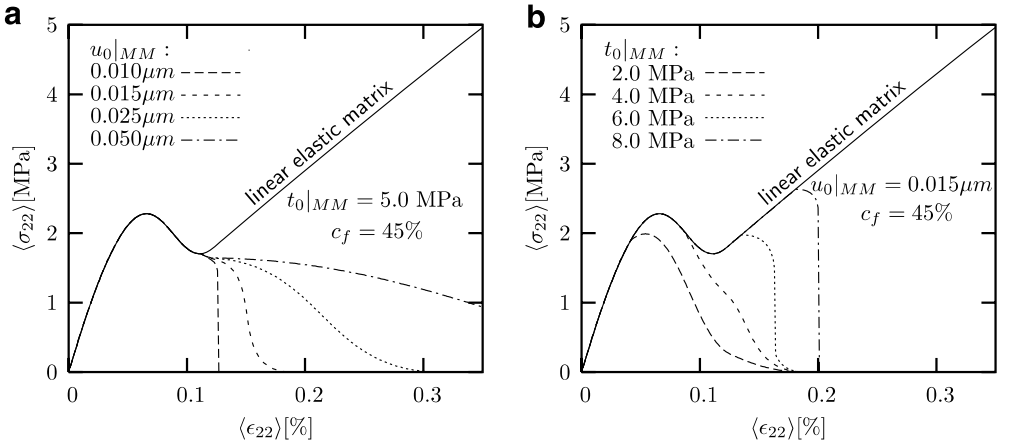

Fig. 11. Stress–strain-curves with matrix cracking. FM-interface parameters $\delta_n|_{\mathrm{FM}} = 0.01$ μm, $\sigma_{\max}|_{\mathrm{FM}} = 2$ MPa. (a) Variation of MM-interface parameter $u_0|_{\mathrm{MM}}$. (b) Variation of MM-interface parameter $t_0|_{\mathrm{MM}}$.

Fig. 12(a) and (b) demonstrate the influence of the damage variables on the stress response $\langle\sigma_{22}\rangle$ during a cyclic transverse loading process $\langle\epsilon_{22}\rangle$ – see Fig. 13. In the range of positive stress the unloading paths of the hysteresis-curves follow the secant through the origin and the point belonging to the attained maximum of the macroscopic strain. Further accumulation of damage only occurs if the former maximum positive strain is surpassed under reloading conditions. In the case of Fig. 12(a) the fibre/matrix bond is assumed to possess an initial compliance. Hence, the compressive material behaviour is different from the tension behaviour with respect to the initial tangential stiffness. This is not the case with the example of Fig. 12(b) where the interface is perfectly bonded unless the normal stress at the fibre/matrix interface reaches the threshold $t_0|_{\mathrm{MM}}$. In both cases the overall compressive stiffness is independent of the damage variables as all the gaps have closed under compression.

Fig. 14(a) and (b) illustrate the stress responses $\langle\sigma_{12}\rangle$ to the cyclic shear deformation process with an increasing amplitude of $\pm\langle\epsilon_{12}\rangle$ – see Fig. 15. The initial compliance of the fibre/matrix bond is unequal to zero in case (a) and equal to zero in case (b). In contrast to the transversal strain process the accumulation of damage is not constrained to a positive sign of the shear strain. The evolution of the stress under unloading or reversed loading conditions proceeds along the direction of the secant defined by the origin of the stress–strain-space and the stress attained at $\max|\langle\epsilon_{21}(\tau)\rangle|$ in past times $\tau \leqslant t$. The evolution of damage only progresses if $|\langle\epsilon_2(t)\rangle|$ exceeds $\max|\langle\epsilon_{21}(\tau)\rangle|_{0\leqslant\tau\leqslant t}$.

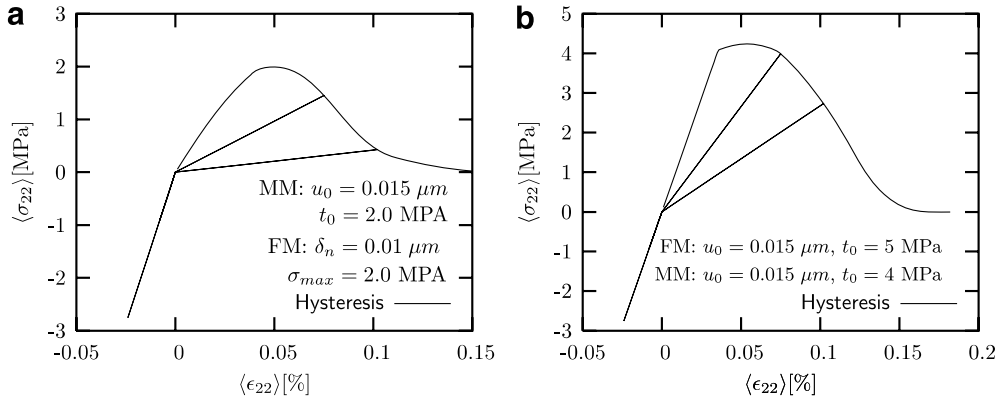

Fig. 12. Hysteresis loops $\langle\sigma_{22}\rangle$ vs. $\langle\epsilon_{22}\rangle$. Debonding and matrix cracking: (a) FM-interface with initial compliance and (b) FM-interface without initial compliance.

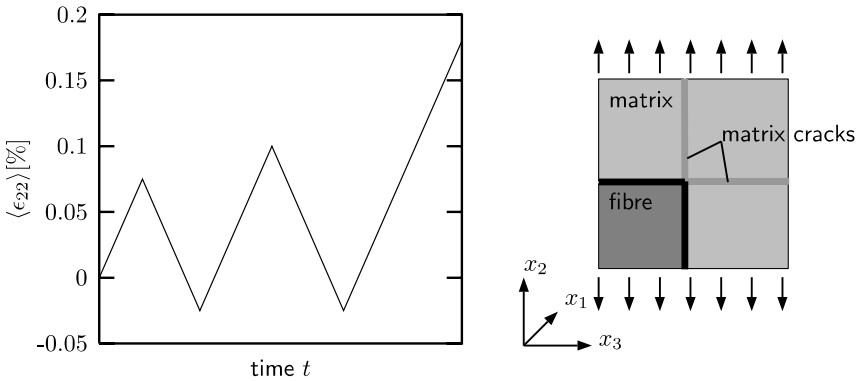

Fig. 13. Transversal strain process $\langle\epsilon_{22}(t)\rangle$ applied to the four subcell model with two debonding fibre/matrix interfaces and two discrete matrix cracks.

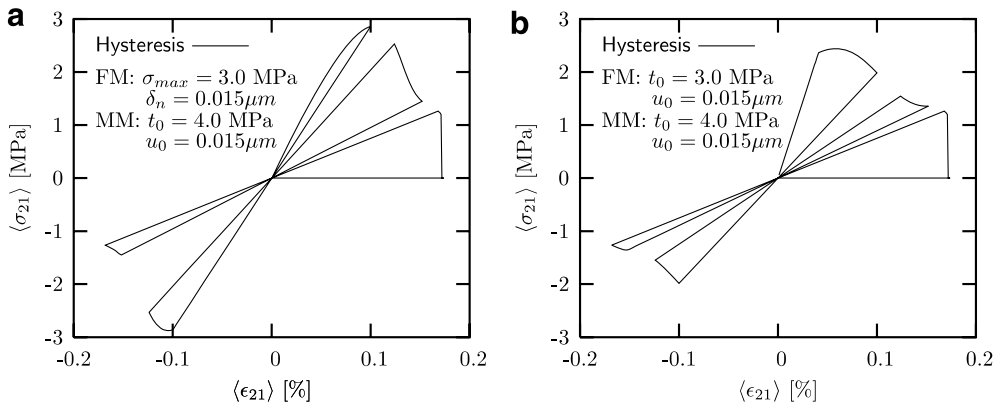

Fig. 14. Hysteresis loops $\langle\sigma_{21}\rangle$ vs. $\langle\epsilon_{21}\rangle$. Debonding and matrix cracking: (a) FM-interface with initial compliance and (b) FM-interface without initial compliance.

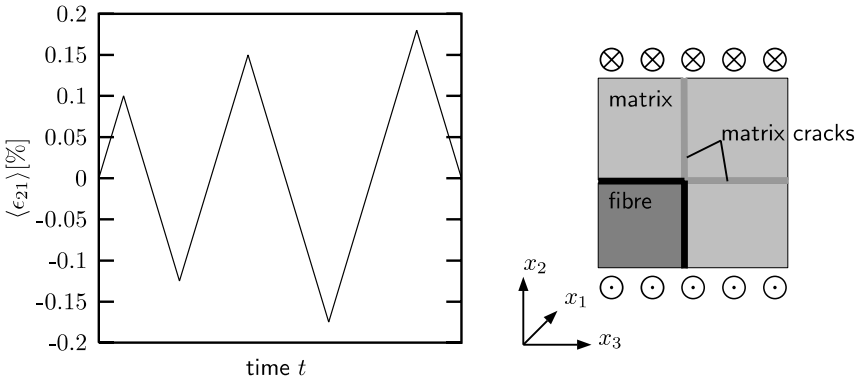

Fig. 15. Axial strain process $\langle \epsilon_{21}(t) \rangle$ applied to the four subcell model with two debonding fibre/matrix interfaces and two discrete matrix cracks.

5. Concluding remarks

The reformulated version of the *Generalized Method of Cells* was used to predict the macroscopic behaviour of unidirectionally reinforced composites. Attention was focused on how an occurring irreversible, nonlinear damage of the fibre–matrix-bond as well as the initiation and growth of matrix cracks influences the effective tangential constitutive tensor and macroscopic stress responses. Therefore, a discontinuous microscopic displacement field was considered. The constitutive equations that correlated the interface tractions with the displacement jumps were based on formulations taken from the literature. The tangential effective stiffness matrix, mapping the rates of the macrostrains to the rates of the macrostresses, was derived. Finally, the GMC was applied to calculate the average stress response and tangential stiffness to strain driven loadings of the representative volume element.

The validation of the cells model described above, that is the comparison of the proposed material responses with those obtained from experimental investigations, is the essential task of future work. As a preliminary to this the identification of the various interface parameters has to be done. Operational experience of the author referring to parameter identification, especially in the context with the method of cells, is discussed in Matzenmiller and Gerlach (in press). Experimental data are available from the so called *World Wide Failure Exercise*, see Soden and Hinton (1998) and Hinton et al. (1998). Since epoxy resins are known to behave nonlinearly elastic under shear loading, it is intended to implement a nonlinear elastic constitutive model for the matrix phase prior to extensive interface parameter identification [see e.g. Hahn and Tsai (1973) or the Ramberg-Osgood nonlinear stress–strain equations used by Aboudi (1991, p. 168)].

Acknowledgement

The financial support of the *Deutsche Forschungsgemeinschaft*, DFG, under contract MA1186/2 is gratefully acknowledged.

Appendix A

It is assigned one number $\kappa = 1, \ldots, 2N_\beta N_\gamma$ to each subcell interface ${}^{(i)}I^{(\beta\gamma)}$ of the GMC-model and a second number $\iota = 1, N_I$ to the ones out of them, which are either imperfectly bonded or cracked. If the interface κ is cracking or debonding (i.e. $\iota \neq 0$), the logical variable $\varepsilon(\iota, \kappa)$ is set $+1$, otherwise $\varepsilon(\iota, \kappa)$ is equal to -1.

For 2×2 subcells and 2 softening interfaces ${}^{(2)}I^{(11)}$ and ${}^{(2)}I^{(11)}$ – see Fig. 2 – the assignment is given by Table 1. The incidence matrix $\mathbb{ID}$ is defined as

$$\mathbb{ID}^q = [\mathbb{D}_{\iota\kappa}] = \begin{bmatrix} \mathbf{1} & \mathbf{0} & \mathbf{0} & \mathbf{0} & \mathbf{0} & \mathbf{0} & \mathbf{0} & \mathbf{0} \\ \mathbf{0} & \mathbf{0} & \mathbf{0} & \mathbf{0} & \mathbf{1} & \mathbf{0} & \mathbf{0} & \mathbf{0} \end{bmatrix} \tag{96}$$

Table 1
Coincidence of GMC-subcell boundaries numbered by κ and debonding/cracking interfaces numbered by ι

Interface	${}^{(2)}I^{(11)}$	${}^{(2)}I^{(21)}$	${}^{(2)}I^{(12)}$	${}^{(2)}I^{(22)}$	${}^{(3)}I^{(11)}$	${}^{(3)}I^{(21)}$	${}^{(3)}I^{(12)}$	${}^{(3)}I^{(22)}$
κ	1	2	3	4	5	6	7	8
ι	1	0	0	0	2	0	0	0
$\varepsilon(\iota,\kappa)$	+1	−1	−1	−1	+1	−1	−1	−1

by the help of the submatrices $\mathbb{D}_{\iota\kappa}$

$$\mathbb{D}_{\iota\kappa} = \begin{cases} \mathbf{1} & \text{if } \varepsilon(\iota,\kappa) = +1 \\ \mathbf{0} & \text{if } \varepsilon(\iota,\kappa) = -1 \end{cases} \tag{97}$$

with the 3×3 unity and zero matrices $\mathbf{1}$ and $\mathbf{0}$. The incidence matrix $\mathbb{ID}^q$ for the damage variable q is given as

$$\mathbb{ID}^q = [\mathbb{D}^q_{\iota\kappa}] = \begin{bmatrix} 1 & 0 & 0 & 0 & 0 & 0 & 0 & 0 \\ 0 & 0 & 0 & 0 & 1 & 0 & 0 & 0 \end{bmatrix} \tag{98}$$

with

$$\mathbb{D}^q_{\iota\kappa} = \begin{cases} 1 & \text{if } \varepsilon(\iota,\kappa) = +1 \\ 0 & \text{if } \varepsilon(\iota,\kappa) = -1 \end{cases} \tag{99}$$

References

Aboudi, J., 1991. Mechanics of Composite Materials – A Unified Micromechanical Approach, first ed. Elsevier, Amsterdam.

Aboudi, J. 1993. Constitutive behavior of multiphase metal matrix composites with interfacial damage by the generalized cells model. In: Voyiadjis, G.Z. (Ed.), Damage in Composite Materials, pp. 3–22.

Aboudi, J., Herakovich, C.T., 1996. An interfacial damage model for titanium matrix composites. In: Damage and Interfacial Debonding in Composites. Elsevier Science, pp. 149–165.

Aboudi, J., Pindera, M.-J., 2004. High-fidelity micromechanical modeling of continuously reinforced elastic multiphase materials undergoing finite deformations. Mathematics and Mechanics of Solids 9, 599–628.

Aboudi, J., Pindera, M.J., Arnold, S.M., 2002. High-fidelity generalization method of cells for inelastic periodic multiphase materials. National Aeronautics and Space Administration NASA/TM-2002-211469.

Bansal, Y., Pindera, M.-J., 2005. A second look at the higher-order theory for periodic multiphase materials. Journal of Applied Mechanics 72, 177–195.

Bednarcyk, B.A., Arnold, S.M., 2000a. A new local debonding model with application to the transverse tensile and creep behavior of continuously reinforced titanium composites. National Aeronautics and Space Administration. Technical Memorandum NASA/TM-2000-210029.

Bednarcyk, B.A., Arnold, S.M., 2000b. A new local failure model with application to the longitudinal tensile behavior of continuously reinforced titanium composites. National Aeronautics and Space Administration. Technical Memorandum NASA/TM-2000-210027.

Bednarcyk, B.A., Arnold, S.M., Aboudi, J., Pindera, M.-J., 2004. Local field effects in titanium matrix composites subject to fibre–matrix debonding. International Journal of Plasticity 20, 1707–1737.

Chaboche, J.L., Glrad, R., Schaff, A., 1997. Numerical analysis of composite systems by using interphase/interface models. Computational Mechanics 20, 3–11.

Hahn, H.T., Tsai, S.W., 1973. Nonlinear elastic behavior of unidirectional composite laminae. Journal of Composite Materials 7, 102–118.

Hill, R., 1963. Elastic properties of reinforced solids: some theoretical principles. Journal of the Mechanics and Physics of Solids 11, 357–372.

Hinton, P.D., Soden, M.L., Kaddour, A.S., 1998. Lamina properties, lay-up configurations and loading conditions for a range of fibre-reinforced composite laminates. Composites Science and Technology 58, 1011–1022.

Lissenden, C.J., 1996. An approximate representation of fibre–matrix debonding in nonperiodic metal matrix composites. In: Voyiadjis, G. (Eds.), Damage and Interfacial Debonding in Composites, pp. 189–212.

Lissenden, Cliff J., 1999. Fibre–matrix interfacial constitutive relations for metal matrix composites. Composites Part B: Engineering 30, 267–278.

Matzenmiller, A., Gerlach, S., 2002. Micromechanical modeling of viscoelastic fiber–matrix bond in composites. In: Mang, H.A., Rammerstorfer, F.G., Eberhardsteiner, J. (Eds.), Proceedings of the Fifth World Congress on Computational Mechanics (WCCM V), 7–12 July 2002, Vienna, Austria. Vienna University of Technology, Austria.

Matzenmiller, A., Gerlach, S., 2004. Micromechanical modelling of viscoelastic composites with compliant fiber–matrix bonding. Computational Materials Science 29 (3), 283–300.

Matzenmiller, A., Gerlach, S. in press. On parameter identification for material and microstructural properties. GAMM (Gesellschaft für angewandte Mathematik und Mechanik) in ZAMM-Mitteilungen.

Needleman, A., 1987. A continuum model for void nucleation by inclusion debonding. Journal of Applied Mechanics 54, 525–531.

Needleman, A., 1991. Micromechanical modelling of interfacial decohesion. Ultramicroscopy 40 (1992), 203–214.

Pindera, M.-J., Bednarcyk, B.A., 1999. An efficient implementation of the generalized method of cells for unidirectional, multi-phased composites with complex microstructures. Composites Part B: Engineering 30, 87–105.

Soden, M.L., Hinton, P.D., 1998. Predicting failure in composite laminates: the background to the exercise. Composites Science and Technology 58, 1001–1010.

Tvergard, V., 1990. Effect of fibre debonding in a Whisker-reinforced metal. Material Science and Engineering A 125, 203–213.